Surface displacements resulting from magma-chamber roof subsidence, with application to the 2014-2015 Bardarbunga-Holuhraun volcanotectonic episode in Iceland

John Browning and Agust Gudmundsson

Royal Holloway University of London, Department of Earth Sciences, Egham TW20 0EX

Contact email: john.browning.2012@live.rhul.ac.uk

Abstract

The conditions which lead to caldera collapse are still poorly constrained. As there have only been four, possibly five, well-documented caldera forming events in the past century, the geodetic signals produced during chamber roof subsidence, or chamber volume reduction (shrinkage) in general, are not well documented or understood. In particular, when two or more geodetic sources are operating and providing signals at the same time, it is important to be able to estimate the likely contribution of each. Simultaneous activities of different geodetic sources are common and include pressure changes in magma chambers/reservoirs occurring at the same time as dyke emplacement. Here we present results from numerical models designed to simulate the subsidence of a magma-chamber roof, either directly (chamber shrinkage) or through ring-fault displacement, and the induced surface deformation and crustal stresses. We consider chamber depths at 3 km, 5 km, and 7 km below the crustal surface, using both non-layered (isotropic) and layered (anisotropic) crustal models. We also model the effects of a caldera lake and of a thick ice cover (ice sheet) on top of the caldera. The results suggest that magma-chamber roof subsidences between 20 m and 100 m generate large (tens of centimetres) vertical and, in particular, horizontal displacements at the surfaces of the ice and the crust out to distances of up to tens of kilometres from the caldera/chamber centre. Crustal layering tends to reduce, but increasing chamber

depth to enlarge, the horizontal and vertical surface displacements. Applying the results to the ice subsidence in the Bardarbunga Caldera during the 2014-2015 Bardarbunga-Holuhraun volcanotectonic episode indicates that the modelled ice displacements are less than those geodetically measured. Also, the geodetically measured crustal displacements are less than expected for a 60 m chamber-roof subsidence. The modelling results thus suggest that only part of the ice subsidence is due to chamber-roof subsidence, the other part being related to flow in the ice. We show that such a flow is likely within the caldera as a result of the stress induced by the 45-km-long regional dyke emplaced (primarily in vertical magma flow) during the episode. This conclusion is further supported by the model results suggesting that the ring-fault (piston-like) displacements must have been much less than the total 60 m ice subsidence, or else faults with tens-of-metres displacements would have cut through the ice (these are not observed). We suggest that the ring-fault subsidence was triggered by small doming of the volcanic field and system hosting the Bardarbunga Caldera and that this doming occurred as a result of magma inflow and pressure increase in a deep-seated reservoir. The doming is confirmed by GPS measurements and supported by the seismicity results. The magmatic pressure increase in the reservoir was, in terms of the present model, responsible for the regional dyke emplacement, the Holuhraun eruption, and part of the stress concentration around, and displacement of, the Bardarbunga Caldera.

Keywords: surface deformation, surface stresses, magma chambers, caldera collapse, Bardarbunga-Holuhraun

1. Introduction

Caldera collapses are a common occurrence in the evolution of major volcanic systems (Fig. 1). Whilst many of these events are catastrophic and associated with the expulsion of large volumes of magma and ignimbrite formation (Druitt and Sparks, 1984), perhaps the more prevalent situation involves relatively small or no magma expulsion (MacDonald, 1965). Well-documented caldera collapses occurred in 2000 and 2007 at the summits of Miyakejima (Geshi et al., 2002) and Piton de la Fournaise (Peltier et al., 2008). These events have been referred to as periodic (Geshi et al., 2002; Michon et al., 2011) or slow collapses. These terms relate to the total caldera growth occurring over periods of perhaps as much as one month (Geshi et

al., 2002). Much of the longer-period caldera growth was due to mass wasting, a process which likely also shaped lake Öskjuvatn (Iceland) following the 1875 caldera forming eruption (Hartley and Thordarsson, 2012). A mechanism of 'slow caldera collapse' has also been suggested as an explanation for the measured ice subsidence during the 2014-2015 Bardarbunga episode (Riel et al., 2015; Sigmundsson et al., 2015).
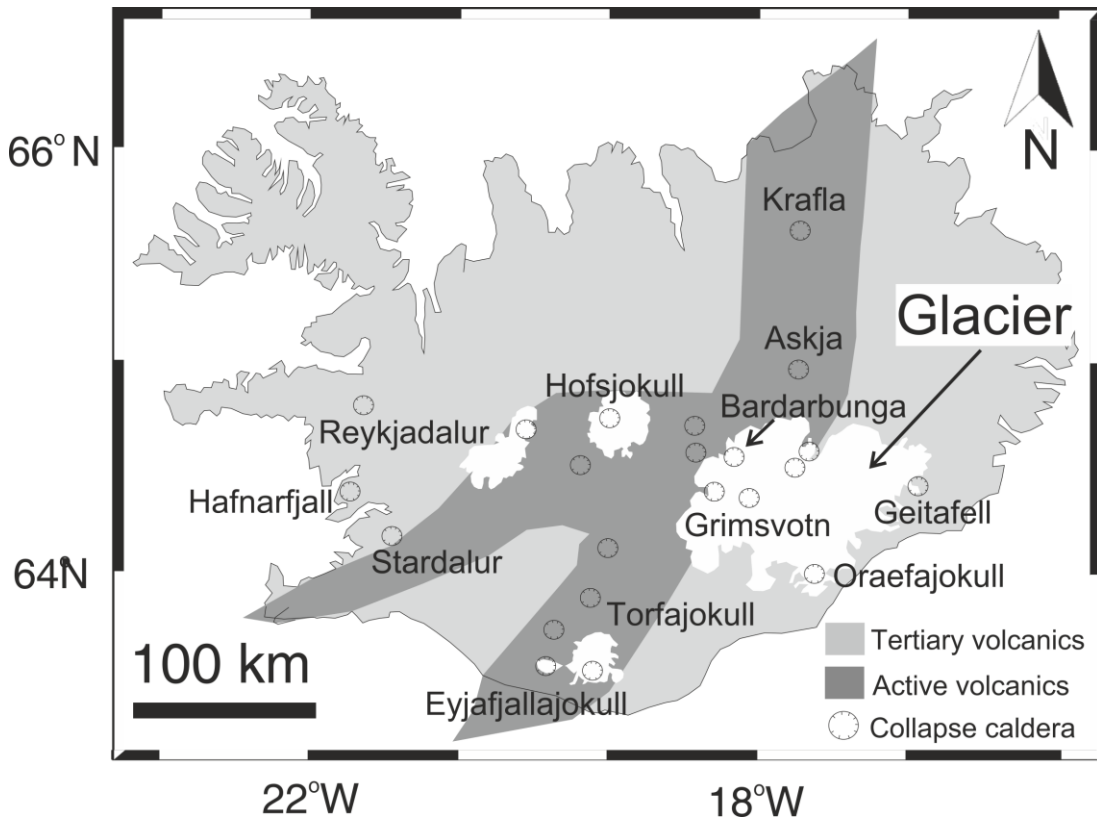

Fig. 1 Simplified geological map of Iceland, showing the main active and inactive volcanoes that contain collapse calderas. Many of these calderas are fully or in part sub-glacial, that is located underneath a body of ice. Glacier outlines are highlighted in this map as white areas.

The timescale of deformation at calderas ranges from events of hours to days (Stix and Kobayashi, 2008) to longer events taking months or years (Hartley and Thordarsson, 2012) as well as cyclic inflation and deflation over tens, hundreds and probably thousands of years (Phillipson et al., 2013). Collapse may occur along pre-existing structures, such as regional faults or earlier-formed ring-faults (Fig. 2), but the shape and size of collapse is significantly influenced by the depth, size, and shape of an underlying magma chamber (Acocella, 2007; Cole et al., 2005).

The movement of large crustal segments, as occurs during the formation or reactivation of collapse calderas, must produce significant crustal deformation. However, the magnitude and type of the deformation is poorly constrained. This is partly due to the lack of geophysical measurements syn-collapse, the exceptions being Piton de la Fournaise (Peltier et al., 2008) and Miyakejima (Geshi et al., 2002), although measurements at these locations were predominantly limited to the central edifice and vent area. Therefore, understanding the far-field effects of crustal subsidence due to caldera formation or chamber shrinkage are useful for constraining geophysical observations at volcanoes where the summit region cannot be observed, either due to cloud cover, inaccessibility, or ice cover. The last point is salient because many, if not most, of the central volcanoes in Iceland are ice covered (Figs. 1 and 3). In addition, understanding the timing and development of collapse is important for hazard and risk estimation, partly because many calderas are associated with the formation of ring-dikes (Fig. 2) (Browning and Gudmundsson, 2015) and give rise to large eruptions (Gudmundsson, 2015).

When magma leaves or flows out of a chamber/reservoir during an eruption and/or dyke injection, the volume of the chamber/reservoir decreases. The same may happen during caldera collapse (Gudmundsson, 2014, 2015). The volume decrease or shrinkage affects the crustal segment hosting the chamber, primarily through changes in stress and associated displacement and strain. The effects of chamber shrinkage are most easily detected through surface deformation. The aim of this work is to understand better a) how the surface deformation associated with chamber shrinkage, in particular during roof subsidence, is reflected in horizontal and vertical displacements (and stresses) at the surface of the hosting crustal segment (as well as at the surface of the ice cover), b) how the surface deformation changes with distance from the chamber, and c) how much surface deformation can feasibly be accommodated in an elastic crust before ring-faults will form or reactivate, resulting in a normal caldera collapse. The results, while completely general, are here applied to the 2014-15 Bardarbunga-Holuhraun volcano-tectonic episode.
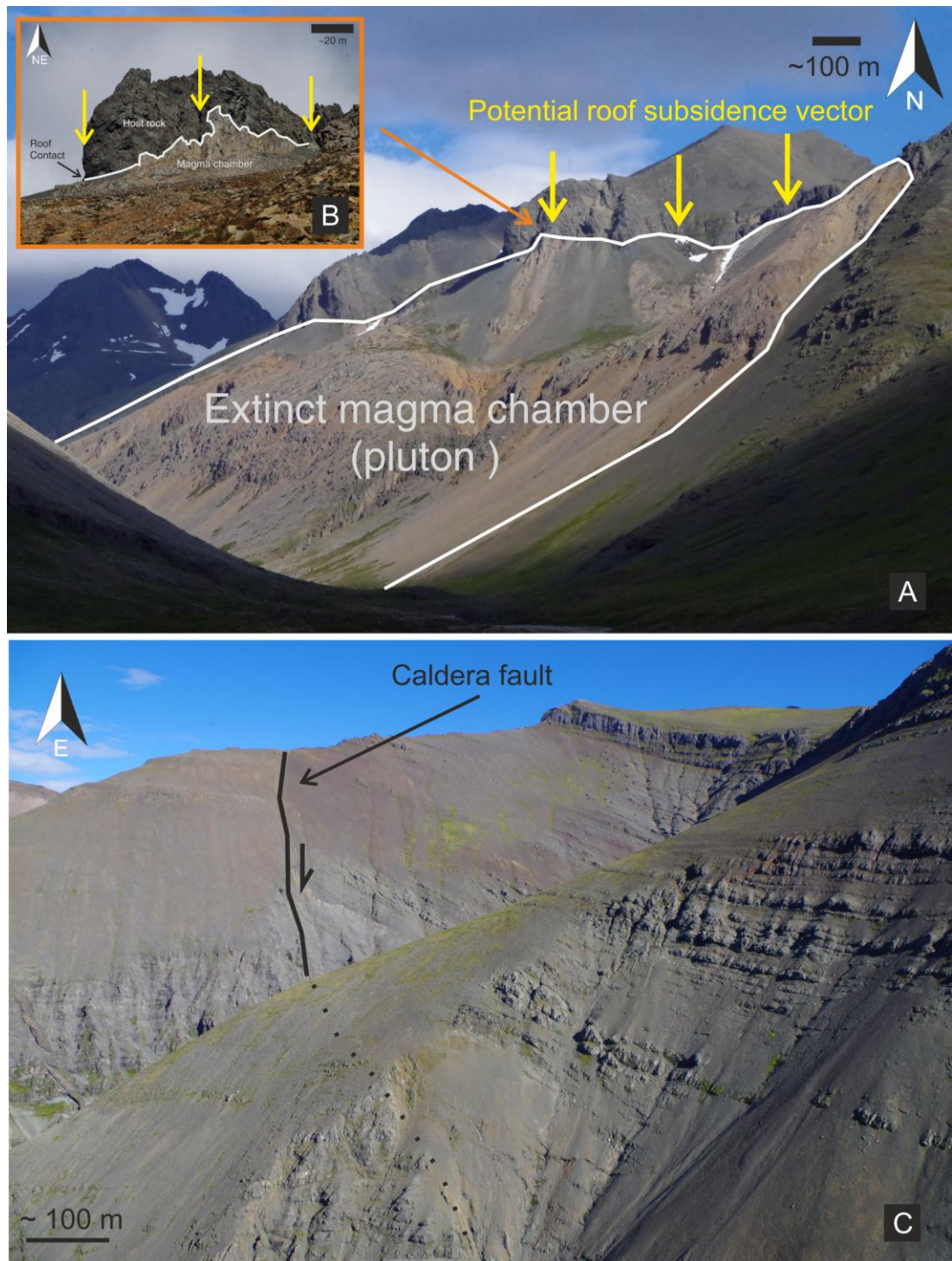
Fig. 2 Exposed sections of extinct central volcanoes in the Tertiary volcanic regions of East (A, B) and West (C) Iceland. An extinct - and now well exposed - granophyre magma chamber at Slaufrudalur in East Iceland. The exposure shows the contact (inset) between the granophyre plutonic rocks at the base of the picture and the basaltic lava pile at the top of the picture, into which the chamber was originally emplaced. Shallow chambers such as this one commonly gives rise to a vertical collapse, culminating in the formation of a surface caldera. Although no evidence exists for a collapse at Slaufrudalur, many eroded central volcanoes in Iceland show clear ring-faults, perhaps the best example being Hafnarfjall in West Iceland (C).

## 2. Stress fields controlling caldera formation

Many analogue models of caldera collapse indicate initial ground surface slumping (Lavallée et al., 2004) followed by the formation of peripheral faults that ultimately control the majority of vertical subsidence (Acocella et al., 2000; Acocella, 2007; Geyer et al., 2006; Holohan et al., 2005; Kennedy et al., 2004). As many of these models use dry sand or other similar granular materials to simulate the crust, it is often impossible to determine surface displacements far from the deformation centre. This follows partly because a dry sand pack lacks cohesion (which corresponds to rock tensile strength) and normally does not transmit tensile stresses as solid linear elastic material. By contrast, the crust behaves approximately as linear elastic solid material with a non-zero tensile strength. More specifically, the range of in-situ tensile strength of solid rocks is 0.5-9 MPa, the most common values being 2-4 MPa (Gudmundsson, 2011). Numerical models which simulate an elastic crustal segment hosting a magma chamber therefore provide a reasonable approximation of surface ground deformation (De Natale and Pingue, 1993; Hickey and Gottsmann, 2014).

In order for a caldera to form, or for slip to occur on a pre-existing ring-fault, there must be suitable state of stress within the crust. The initiation of sub-vertical, normal ring-faults depends on three stress field conditions which must be satisfied simultaneously (Gudmundsson, 1998; Folch and Marti, 2004).

1. The minimum value of σ_3, the maximum tensile (minimum compressive) principal stress, must be at the surface.

2. The maximum value of $(\sigma_1-\sigma_3)/2$, the shear stress, must occur above the outer margins or lateral edges of the magma chamber, that is, in a zone extending from the lateral edge of the chamber to the surface and within which the ring-fault forms (or slips).

3. The maximum tensile stress at the surface must peak at a radial distance approximately equal to the lateral dimension, the diameter, of the magma chamber.

These stress conditions are most likely to be induced by a double magma chamber, where the shallow chamber is sill-like and (a) the crustal segment hosting the double chamber is subject to horizontal extension, or (b) the deeper chamber, a large

reservoir, is subject to slight increase in magma pressure so as to dome the crustal segment hosting the shallower chamber (Gudmundsson, 1998, 2007) (Fig.3). Other predominant collapse trigger mechanisms (Marti et al., 2009) include (i) internal magma chamber overpressures initiating roof and surface fractures (e.g., Gudmundsson, 1998; Gray and Monaghan, 2004; Gudmundsson, 2007; Gregg et al., 2012) and (ii) internal magma chamber underpressure following chamber rupture (e.g., Roche et al., 2000; Folch and Marti, 2004; Geyer et al., 2006; Kusumoto and Gudmundsson, 2009; Hologhan et al., 2011). Here we consider in detail a situation more compatible with the second of these two mechanisms, namely an inferred underpressure in the shallow chamber, particularly in view of the suggestions that the ice subsidence during the Bardarbunga-Holuhraun episode being related to pressure decrease in the chamber (e.g., Riel et al., 2015; Sigmundsson et al., 2015).
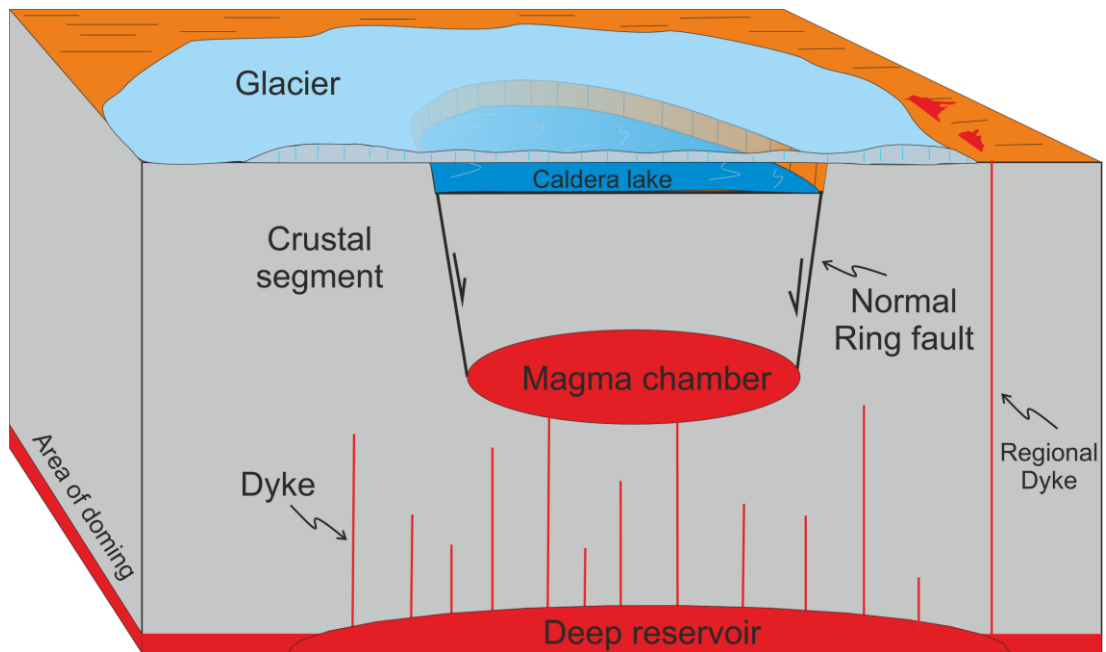

Fig. 3 Sub-glacial caldera occupied by a caldera lake. Here the ring-fault is a normal fault, as is inferred for nearly all collapse calderas in Iceland (Bjarnason, 2014), including the Bardarbunga Caldera (Riel et al., 2015). The shallow chamber is fed by a much larger deep-seated reservoir that undergoes periods of doming and inflation when receiving new input of melt or magma. In this example the area of doming is much larger than the caldera. Modified after Gudmundsson (2007).

As indicated above, shallow chambers within crustal segments undergoing slight doming, regional extension, or both are the ones most likely to generate stress concentrations favourable for ring-fault formation (Gudmundsson, 2007). Prime examples of this type of regional settings are the volcanoes of the Eastern Volcanic Zone (EVZ) in Iceland (Gudmundsson, 2007), the Kenyan Rift valley (Acocella, 2007) and the Taupo Volcanic Zone (TVZ) in New Zealand (Cole, 1990). Figure 4 shows the stresses around a sill-like magma chamber with negative internal pressure, an underpressure, of 5 MPa (e.g., Folch and Marti, 2004), located at 5 km depth in a 40-km wide and 20-km thick crustal segment but simultaneously subject to excess (doming) pressure of 10 MPa from a deep-seated reservoir. In this example, the doming pressure largely controls the stress/displacement fields and the maximum tensile stress concentrates at the free surface in a zone above the lateral margins or edge of the shallow sill-like chamber. In addition, the maximum shear stress concentrates at the lateral margins of the magma chamber at depth. These conditions are ideal for the formation of, initially, tension fractures at the surface that propagate down towards the chamber and change at a critical depth - normally less than 0.5 km (Gudmundsson (2011) - to normal faults (Gudmundsson 1998; Gray and Monoghan, 2004). If the tensile stresses are higher at the magma chamber margin than at the free surface above the margin, then a ring-dyke would be more likely to form (Gudmundsson, 2007).

When a caldera forms, it is common for the depression to be filled with water, generating in a caldera lake. Well-known examples include Crater Lake, USA (Williams, 1941) and Askja, Iceland (Hartley and Thordarson, 2012) amongst many others (Fig. 3). The occurrence of sub-glacial lakes within calderas has also been noted, such as in the Grimsvötn volcanic system in Iceland (Gudmundsson et al., 1997). A caldera lake is important because the solid contact with water gives rise to a free surface, that is, a surface of zero shear stress. Therefore, a caldera lake will reduce the mechanical coupling between bedrock and glacier which in-turn will influence stresses and displacements within the ice.
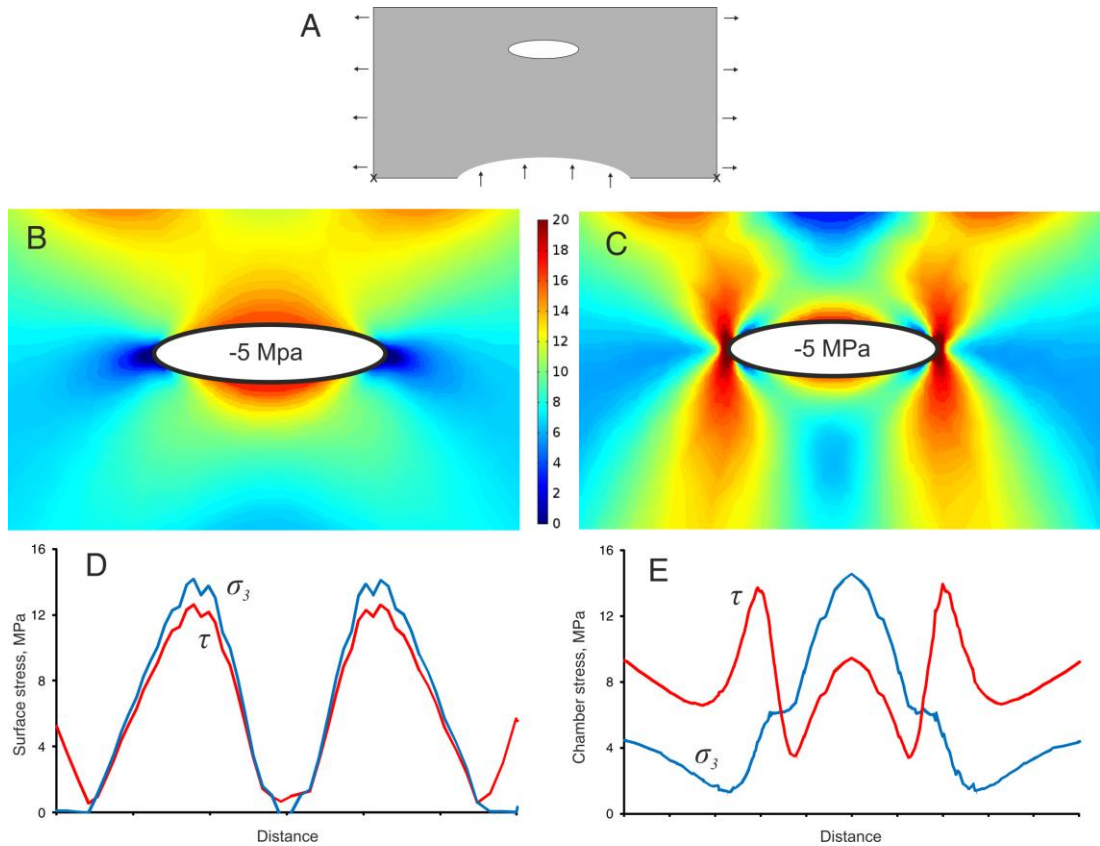
Fig. 4 Stress fields favouring the formation of caldera ring-faults. The stresses shown are generated around a sill-like magma chamber, 8 km wide and 2 km thick, located at 5 km depth in a 20-km-thick and 40-km-wide crustal segment subject to horizontal tensile stress of 5 MPa and doming stress (pressure) from a deep-seated reservoir (at the base of the model) of 10 MPa. Chamber excess pressure is negative (underpressure) 5 MPa and it is hosted within a homogeneous, isotropic crustal segment of stiffness (Young's modulus) 40 GPa and Poisson's ratio of 0.25 (see Table 1). A, model configuration; B, magnitudes of the maximum principal tensile stress σ_3; C, magnitudes of the von Mises shear stress τ; D, maximum principal tensile stress σ_3, and von Mises shear τ stress at Earth's free surface; E, maximum principal tensile stress σ_3, and von Mises shear τ stress around the magma-chamber boundary. Figure C shows clearly that the shear stress concentrates in subvertical zones above the lateral ends of the chamber, thereby encouraging the formation of a subvertical ring-fault.

3. Model set-up

The finite element program Comsol was used to investigate the crustal and ice-sheet response to the vertical displacement of the magma-chamber roof (www.comsol.com; cf. Zienkiewicz, 1979; Deb, 2006). In these models the magma chamber is modelled as a cavity (Gudmundsson, 2011; Grosfils et al., 2013). In the first model the chamber is residing within a homogeneous, isotropic elastic half-space with a Young's modulus (*E*) of 40 GPa and Poisson's ratio (*v*) of 0.25 (Fig. 4).

In this model, the focus is on the typical conditions for ring-fault formation or reactivation in rift-zone environment. Thus, the loading condition is a combination of doming excess pressure of 10 MPa in the deep-seated reservoir and a horizontal tension of 5 MPa. The results are in agreement with earlier results suggesting that doming, horizontal tension, or both are loading conditions that favour the concentration of shear stress in a zone above the lateral ends or edges of the shallow chamber (Fig. 4B). Furthermore, the induced tensile stress peaks where these zones meet the free surface (Fig. 4A). The zones of high shear stress are thus likely to develop ring-faults, for the given loading conditions.

Horizontal tension, however, will not be much discussed here. In the later part of the paper, we discuss the effects of doming by the deep-seated reservoir. The main focus here is on the effects of shallow-chamber roof subsidence on the associated surface deformation and stresses. The roof (upper boundary) of the chamber is supposed to subside, so that, the loading is prescribed negative vertical (z-axis) displacement. The vertical roof displacements tested in the models range from 20 m to 100 m. To make the models realistic, the crustal segment hosting the chamber is also modelled as anisotropic, that is, layered (Fig. 5). In the anisotropic models, directly above the chamber there are six layers, each with thickness t and of varying stiffness (Young's modulus, E) but constant density ($\rho = 2500$ kg/m^3) and constant Poisson's ratio ($v = 0.25$), simulating an anisotropic crust. The number of layers used in the models is arbitrary as most volcanic systems are presumably made of hundreds of layers, while many of these may group into larger units of internally similar mechanical properties. Here we choose to include six layers or units simply to investigate the effects of crustal anisotropy on the local stresses and displacements. The uppermost layer of thickness (*2t*) represents an elastic body of ice; namely a glacier, with a Young's modulus of 4 GPa. We use ice as the top-most layer primarily because many volcanoes are located beneath ice sheets, particularly in Iceland, including recently erupting volcanoes in Iceland such as Bardarbunga (Gudmundsson et al., 2014; Riel et al., 2015; Sigmundsson et al., 2015), Grimsvotn (Gudmundsson et al., 1997), and Eyjafjallajökull (Gudmundsson et al., 2012).
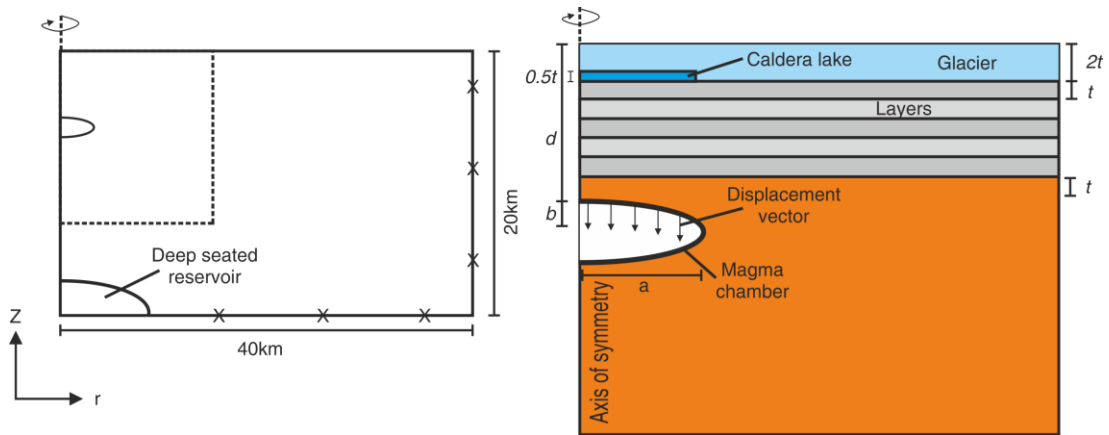
Fig. 5 Sketch of the model setup showing the geometric relationship between a shallow magma chamber within a crustal segment composed of five layers. In some subsequent models (referred to as layered models), the 5 layers have different stiffnesses (Young's moduli), whereas in other models (referred to as non-layered models) all the 5 layers have the same Young's modulus and thus function as a single, thick layer. At the surface of the crust, there is a caldera lake, providing a free surface (surface free of shear stress). In addition, a glacier is on top of the lake and the surrounding crust, the top of the glacial layer is another free surface. All models shown are symmetric with rotation around the z-axis (axi-symmetric), the base and vertical margins are fixed (i.e experience zero displacement). The magma chamber roof is subject to a prescribed vertical displacement between 20 and 100 m. In addition to the shallow magma chamber, several models include a deep-seated reservoir. (Modified after Folch and Marti, 2004, and Kinvig et al., 2009)

For the purpose of this study we model the ice as a brittle layer which behaves elastically through its entire thickness (Geyer and Bindeman, 2011). Other studies assume that only certain parts of an ice layer behave elastically, with the remaining parts behaving as ductile - using, for example Glen's flow law (e.g. Paterson, 1994; Gudmundsson et al., 2004; Schulson and Duval, 2009). Ice behaves elastically for high strain rates and comparatively low stresses or pressures (Schulson and Duval, 2009). The brittle deformation of ice is exemplified in the formation or fractures, crevasses, as are common during subsidence associated with volcanism (Gudmundsson et al., 1997, 2004). The assumption of linear elastic behaviour of the ice is thus reasonable and does not significantly affect the calculated displacements and stresses in the crust (the surface rock) itself outside the ice sheet. The crustal layering or anisotropy is of much greater significance than the assumed elastic behaviour of the ice as regards surface deformation (e.g Manconi et al., 2007; Geyer and Gottsmann, 2010). The mechanical properties of ice are variable (Schulson and

Duval, 2009). For example, typical laboratory values of stiffness or Young's modulus (E) can range from as high as 15 GPa (Gammon et al., 1983; Schulson and Duval, 2009) to more commonly 8-9 GPa, depending on temperature, and grain size and and orientation (Parameswaran, 1987). The stiffness values are only moderately anisotropic (Schulson and Duval, 2009). These are dynamic values, however. Static values are more difficult to measure because of time-dependent deformation in ice. Estimated typical static or field values for Young's modulus of ice are around 1 GPa (Schulson and Duval, 2009). Poisson's ratios for ice are commonly between 0.2 and 0.4 (Schulson and Duval, 2009). In the modelling we use a Young's modulus somewhere between typical field and (dynamic) laboratory values, or 4 GPa. Also, we use a Poisson's ratio of 0.3 and a density of 920 kg m^{-3}. The general crustal and ice parameters used in the numerical models are given in Table 1.

Table 1
Model parameters

Material	Young's modulus (E) (Gpa)	Density (ρ) (kg/m3)	Poisson's ratio (v)
Crust	40	2500	0.25
Glacial Ice	4	920	0.3
Hyaloclastite	1	2500	0.25
Ring fault	0.1	2500	0.25

In all models we assume a strong coupling between glacier and bedrock or crustal surface (except at the location of the caldera lake) using the same assumptions as Geyer and Bindeman (2011). More specifically, if the coupling between the ice and the bedrock is of sufficient strength, stresses within the crust are transmitted to the ice. Then the ice can be considered to act mechanically as part of the layered crust. The other mechanical situation is where the ice and crust are weakly bonded, in which case slip may occur along the weak boundary and stresses would not be transferred from the bedrock surface to the ice. We consider one such scenario where the ice and crust are not directly coupled, designed to represent a caldera lake. The lake depth is *0.5t* (half the thickness of a typical crustal layer) and its width is *a* (the radius of the magma chamber/caldera). The lake is modelled as a free surface at all edges. This follows because the contact between water and the bedrock below as well as the contact with the ice above are surfaces of zero shear stress. As previously

stated, many if not most calderas develop a caldera lake at some point, particularly those calderas formed under ice (Fritz et al., 1990).

If the stresses within a volcano are suitable for the formation of a caldera then displacement would be likely to occur along a bounding ring-fault (circumferential fault). In order to incorporate the mechanical response to ring-faulting we include in one of the models a soft (low-Young's modulus) vertical zone directly above the magma-chamber edge. This zone is supposed to represent a typical caldera fault, a ring-fault (without a ring-dyke) consisting of a highly fractured and mechanically soft damage zone with respect to the host rock (Browning and Gudmundsson, 2015). The magnitudes of the vertical and horizontal displacements depend on the magma chamber size - in this case the chamber radius a is 4 km (its horizontal diameter thus 8 km). All models assume uniform vertical displacement of the roof, that is, a piston-like subsidence irrespective of the absence (as in most models) or the presence (as in one model) of the ring-fault itself.

4. Comparison of numerical and analytical solutions

Periods of unrest are often characterised by surface inflation or deflation of the volcano. This deformation signal is commonly explained in terms of a magmatic excess pressure change (p_e) in the associated magma chamber of radius a and depth d below the surface, modelled as a nucleus of strain. In volcanology, such a nucleus is normally referred to as the "Mogi model" (Mogi, 1958; Fig.6), although the nucleus-of-strain solution with application to volcanoes was initially derived by Anderson (1936). Mogi's analytical solution can be replicated using the finite element method (e.g., Masterlark, 2007; Hickey and Gottsman, 2014). If a Poisson's ratio of 0.25 is assumed for the elastic half-space – generally a reasonable assumption – then the basic equations of the Mogi (1958) can be presented as follows:

$$u_z = \frac{3p_e a^3 d}{4\mu(r^2 + d^2)^{3/2}} \qquad (1)$$

$$u_r = \frac{3p_e a^3 r}{4\mu(r^2 + d^2)^{3/2}}$$ (2)

where u_z and u_r are the vertical and horizontal (radial) displacements at the surface above the magma chamber, respectively. Also, p_e is the magmatic excess pressure in the chamber, a is the radius of the chamber, μ is shear modulus, d is the depth to the centre of the chamber below the surface of the earth (Fig. 6), and r is the radial coordinate at the surface. At the point right about the centre of the magma chamber, we have $r = 0$, and the maximum vertical displacement u_z becomes (Fig. 6):

$$u_z = \frac{3p_e a^3}{4\mu d^2}$$ (3)

Magmatic underpressure, that is, pressure less than lithostatic, is often regarded as the condition for ring-fault and ring-dyke formation. In fact, an underpressure or contracting nucleus-of-strain was Anderson's (1936) original model for the formation of ring-dykes and the connection with the Mogi model is straightforward (cf. Kusumoto and Gudmundsson, 2009).
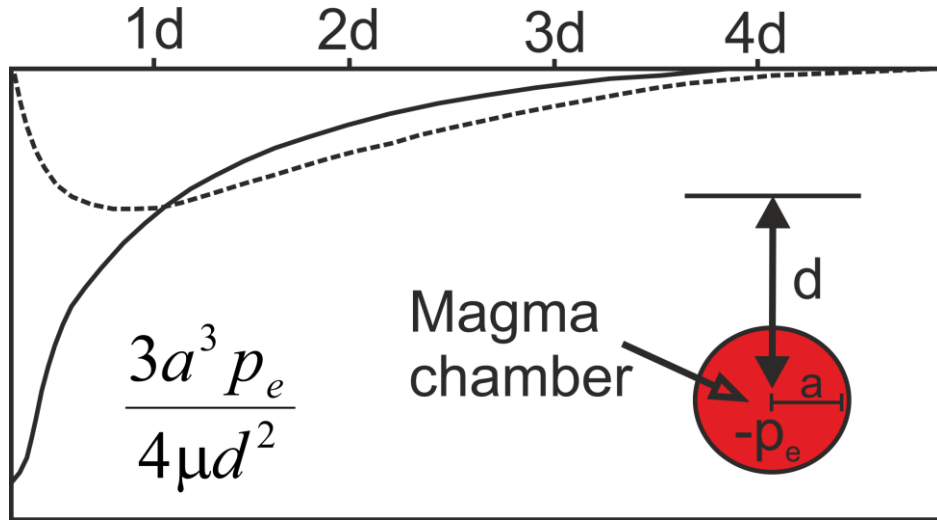
**Fig. 6** Point-pressure source, a nucleus of strain, referred to as the Mogi model in volcanology. Such a model is commonly used for explaining surface deformation above an assumed spherical magma chamber. The solid curve gives the vertical surface displacement, which is maximum above the chamber centre. The dashed curve gives the horizontal surface displacements. The magma chamber, with radius

(*a*) is subject to negative excess pressure, that is, underpressure (-p_e) and located at a depth (*d*) below the surface. (cf. Eqs. 1-3).

In Fig. 7 we show the numerical results of a two-dimensional (circular) chamber subject to an underpressure of 10 MPa, a common underpressure value when considering ring-fault formation (Geyer et al., 2006; Gudmundsson, 2007; Kusumoto and Gudmundsson, 2009). We model the horizontal and vertical displacement at the surface of the ice and at the surface of the bedrock (the crust under and outside the ice sheet) for two magma-chamber depths: 3 km and 5 km. The modelled chamber radius is 1 km and is thus small in relation to the chamber depth below the surface, as it should be for a "Mogi model". There are two basic model configurations. The first one (Fig. 7A) has no caldera lake, but the second one (Fig. 7B) has a caldera lake between the bottom of the ice and the bedrock surface. The lake is included in several of the models in this paper because, as indicated above, such lakes are common in the many calderas located beneath ice in Iceland (Gudmundsson et al., 1997, 2004, 2012).

The surface displacements, vertical and horizontal, are very small (less than 3 cm) for this type of loading (Fig. 7), suggesting that a 'Mogi model' is, as a rule, not very suitable for generating large (tens-of-metre scale) subsidences. The geometries of the displacement curves (Fig. 7), however, are in excellent agreement with those obtained from the Mogi model (Fig. 6). The displacement results (Fig. 7) are shown both for the surface of the rock (the crust under and outside the ice) as solid lines as well as for the surface of the ice itself, as broken lines. As is also seen in subsequent models, the caldera lake has great effects on the displacement curves for the surface of the ice. The other main results as regards the surface-displacement curves will be discussed in context of the later and more realistic models, to which we turn now.
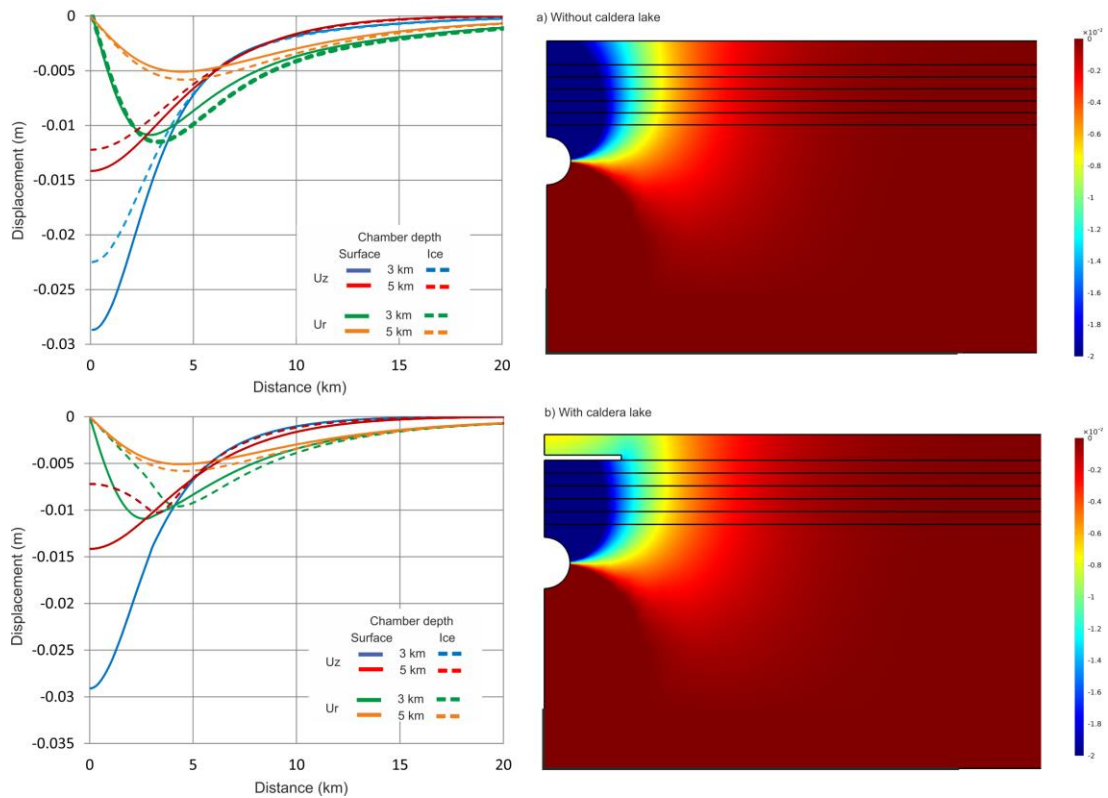
Fig. 7 Crustal surface and ice-surface displacements resulting from negative excess pressure, or depressurisation, of -10 MPa in a circular chamber with a roof at 3 km and 5 km depth below the crustal surface. The upper model (a) shows a homogeneous isotropic crust with an upper ice layer. The lower model (b) also shows a homogeneous isotropic crust but this time incorporates a rectangular free surface, designed to replicate a caldera lake. Total displacement contours are given on the right in metres. The magnitude of displacements in the two models are generally similar, but the displacement patterns differ somewhat, especially in the ice layer.

## 5. Roof subsidence of a sill-like magma chamber

Here we present the results of the stresses and surface displacement induced by a given subsidence of the roof of a sill-like magma chamber. The chamber, modelled as a cavity within a crustal segment, is given a zero excess pressure condition at its lower boundary and prescribed a vertical displacement at the upper boundary in all models apart from those simulating slip on the ring-fault. Thus, in the models the chamber is in lithostatic equilibrium with its surroundings prior to the prescribed vertical displacement, that is, the roof subsidence. While these models are partly "inspired" by the events in Bardarbunga 2014-15, they are completely general and apply to all central volcanoes – collapse calderas in particular – under ice. We explore two main types of models, namely where the magma chamber is located (1)

in a homogeneous, isotropic crustal segment, and (2) in a layered, anisotropic, crustal segment. Based on information from Bardarbunga, where the maximum subsidence of the ice surface is estimated at around 60 m (Hensch et al., 2015), we explore vertical roof displacements or subsidences from 20 m to 100 m. To cover the likely shallow chamber depths, we consider chambers with roofs at depths of 3 km, 5 km, and 7 km below the crustal or rock surface.

5.1 Homogeneous crustal segment

These models are somewhat similar in set-up as the elastic half-space or the Mogi model (Mogi, 1958; Kusumoto and Gudmundsson, 2009; Fig. 7). There are, however, three main differences between the present models (Fig. 8) and the numerical models in Fig. 7. First, the shallow magma chamber (cavity) has here (Fig. 8) a sill- like geometry in contrast to the spherical or point-like Mogi source (circular in Fig. 7). Also, here the radius of the chamber a is 4 km (Fig. 8), and thus 4-times the radius of the previous circular chamber (Fig. 7), and with a maximum thickness $2b$ of 2 km. Second, the displacements at the surface of the bedrock (the crust) and the ice result here from prescribed chamber-roof vertical displacement or subsidence rather than the underpressure in the models in Fig. 7. Third, the subsequent sill-like chamber models analyse chambers in a layered (anisotropic) crustal segment rather than in an elastic half-space as is done in the Mogi model (Fig. 7), and some of the sill-like models also include a lake beneath the ice, thereby forming a free surface.
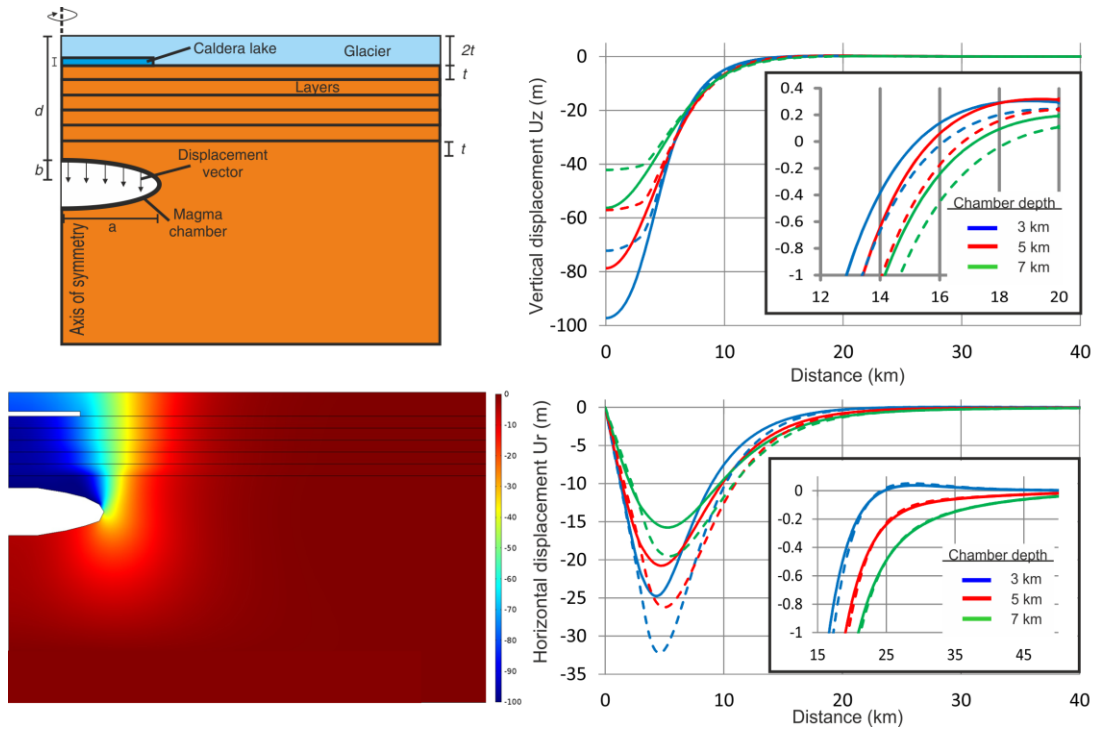
Fig. 8 Vertical and horizontal ground-surface (solid curves) and ice-surface (dashed curves) displacements in metres resulting from a maximum prescribed chamber-roof displacement of 100 m. Here the crust is non-layered. In all model runs the maximum vertical surface displacements of the ice and the crust occur over the chamber centre (in the caldera centre) whereas the maximum horizontal displacements of ice and crust occur around 5 km away from the caldera centre. Vertical crustal surface displacements are larger than the ice displacements, but the opposite is true for the horizontal displacements. Insets display the distances from the chamber where <1 m of vertical and horizontal displacements would be observed. Note that significant (10-20 cm) vertical displacement occurs out to 15 to 16 km from the caldera centre. Similarly, horizontal displacements of 10-20 cm occur out to 30 to 45 km (depending on chamber depth) from the caldera centre. Chamber radius (a) is 4 km and half-thickness (b) is 1 km, depth (d) varies between each model run, as indicated by the separate line colours.

Figure 8 shows the vertical (u_z) and horizontal or radial (u_r) surface displacements of the ice and the bedrock (or crust) resulting from a vertical chamber-roof displacement or subsidence of 100 m. Here there is no ring-fault. The chamber roof is prior to the displacement at different depths below the bedrock or crustal surface d, namely at depths of 3, 5 and 7 km. Salient model results are shown in Table 2, but here we summarise some of the basic results (Fig. 8) as follows:

- The maximum vertical displacement (shown as negative displacement or surface subsidence), both of the ice and the crust, is above the centre of the

18

magma chamber. The subsidence reaches about 97 m in the bedrock/crust and about 78 m in the ice (Table 2). The subsidence changes to uplift or doming at distances of 15-18 km (depending on the chamber depth) from the surface point right above the chamber or caldera centre (Fig. 8). Unless otherwise stated, chamber/caldera centre in the discussion that follows refers to this surface point.

- The maximum horizontal displacement towards the centre (above the centre of the chamber), shown as negative, reaches its maximum at 4-5 km from chamber/caldera centre. The horizontal displacement reaches a maximum of about 25 m in the crust and about 32 m in the ice (Table 2). For the chamber at 3 km depth, however, the horizontal displacement becomes positive (movement away from the centre) at about 25 km distance from the centre.

- The vertical surface displacement, both in the ice and in the bedrock/crust, is less than that of the chamber roof. There is thus not a one-to-one correspondence between the displacement at the surface either of the ice or the crust and the chamber roof subsidence.

- The vertical and horizontal displacements extend to distances far from the chamber/caldera centre. Thus, in both the bedrock/crust and the ice the vertical displacement is in excess of 0.5 m out to distances of about 14 km, whereas the horizontal displacements are in excess of 0.5 m out to distances of about 19 km (Table 2).

Table 2
Model results assuming a 100 m displacement of a chamber roof residing at 3 km

Setup	Uz Max (-m)		Ur Max (-m)		x distance (km) when Uz = 0.5 m		x distance (km) when Ur = 0.5 m	
	Crust	Ice	Crust	Ice	Crust	Ice	Crust	Ice
Homogeneous	97.21	71.75	24.75	32.22	13.8	14.4	18.6	19.1
Heterogeneous A	79.12	64.14	2.3	10.26	12.2	12.3	11.8	14.7
Heterogeneous B	84.14	64.68	5.78	6.92	11.6	11.6	16.9	16.3
Ring-fault	98.5	70.18	23.09	30.31	13.5	14.1	18.4	18.9

Generally, significant surface displacements associated with the chamber-roof subsidence of 100 m occur at lateral distances of up to 40-50 km (in the ice as well as in the bedrock/crust) from the chamber/caldera centre. For example, a chamber located at 3 km depth produces horizontal surface displacements of 20 cm at approximately 21 km from the chamber/caldera centre, whilst a chamber at 7 km

depth produces the same displacement at approximately 33 km from the centre. Thus, for the imposed vertical displacement of the chamber roof, large horizontal displacements are expected out to tens of kilometres from the chamber, and these should be easily detected in the ice or at the bedrock/crustal surface by geodetic measurements.

In the second set of homogeneous crustal models, we consider the effects of a pressurised deep-seated reservoir, such as are common as magma sources for shallow chambers in Iceland (Gudmundsson, 2012) (Fig, 9). Doming is modelled as being the effect of 10 MPa excess magmatic pressure acting on the roof (a boundary load) of the reservoir. The general effect of doming is to reduce the magnitude of vertical and horizontal surface displacements but increase the surface area where those displacements are significant. In other words, the subsidence becomes much less concentrated at the surface immediately above the shallow chamber.
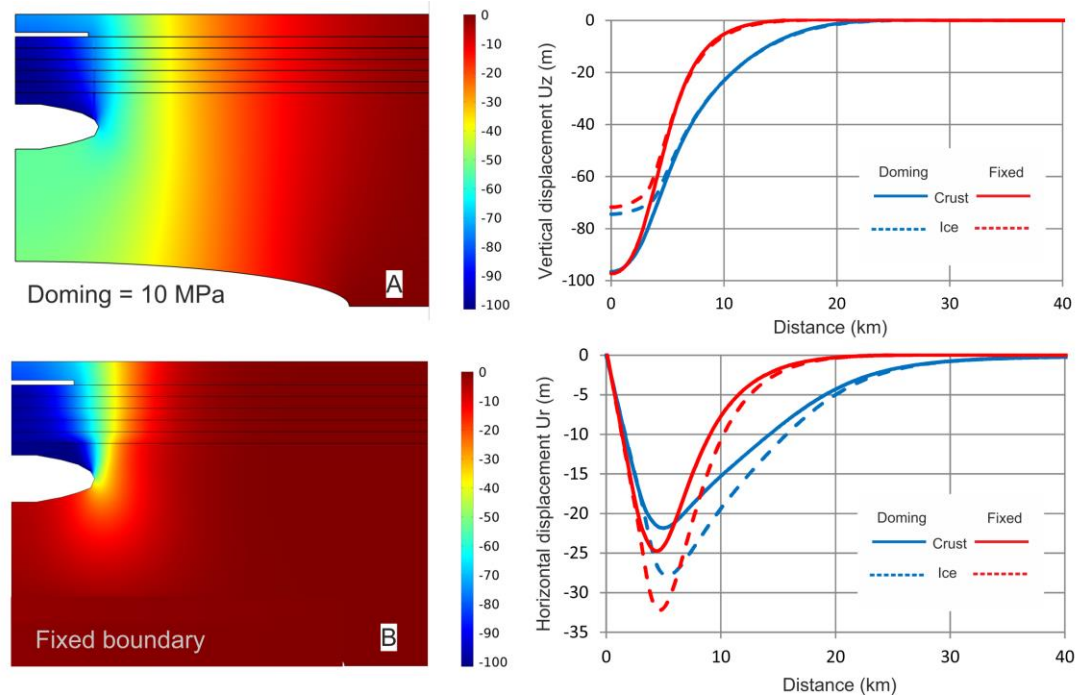
Fig. 9 Vertical and horizontal ground-surface and ice-surface displacements in metres resulting from a maximum prescribed chamber-roof displacement of 100 m, and either a) doming overpressure of 10 MPa in a deep-seated reservoir (blue lines) or b) fixed lower boundary (red lines). Here the crust is non-layered. Doming has the general effect of reducing the maximum horizontal displacement but increasing the radial distance or area over which significant horizontal displacement occurs. Magnitudes of vertical displacement are not greatly affected by doming, but the area of vertical subsidence increases in the absence of a fixed boundary. Shallow chamber

radius (a) is 4 km and half-thickness (b) is 1 km, depth (d) is 3 km. Deep reservoir radius is 16 km with a half-thickness of 2 km at a depth of 10 km.

In the third set of homogeneous crustal models, we added vertical faults (Fig. 10). These are supposed to represent a two-dimensional version of a caldera ring-fault. The fault is modelled as a soft elastic inclusion, that is, as a zone with a low Young's modulus. This is because active or recently active faults have generally lower Young's moduli than most of the host rock because the fault is composed of a fractured damage zone and breccia fault core (Gudmundsson, 2011; Browning and Gudmundsson, 2015). The precise relationship between damage and Young's modulus evolution in caldera settings is, as yet, poorly constrained. The results (Fig. 10) are similar to those of the previous models without a fault (Fig. 8) but differ in that surface subsidence is concentrated within a narrower region around the chamber margin. In addition the crust experiences significant (~30 cm) positive (doming) displacement, measured as an inflation signal between approximately 15 km and 20 km from the centre.
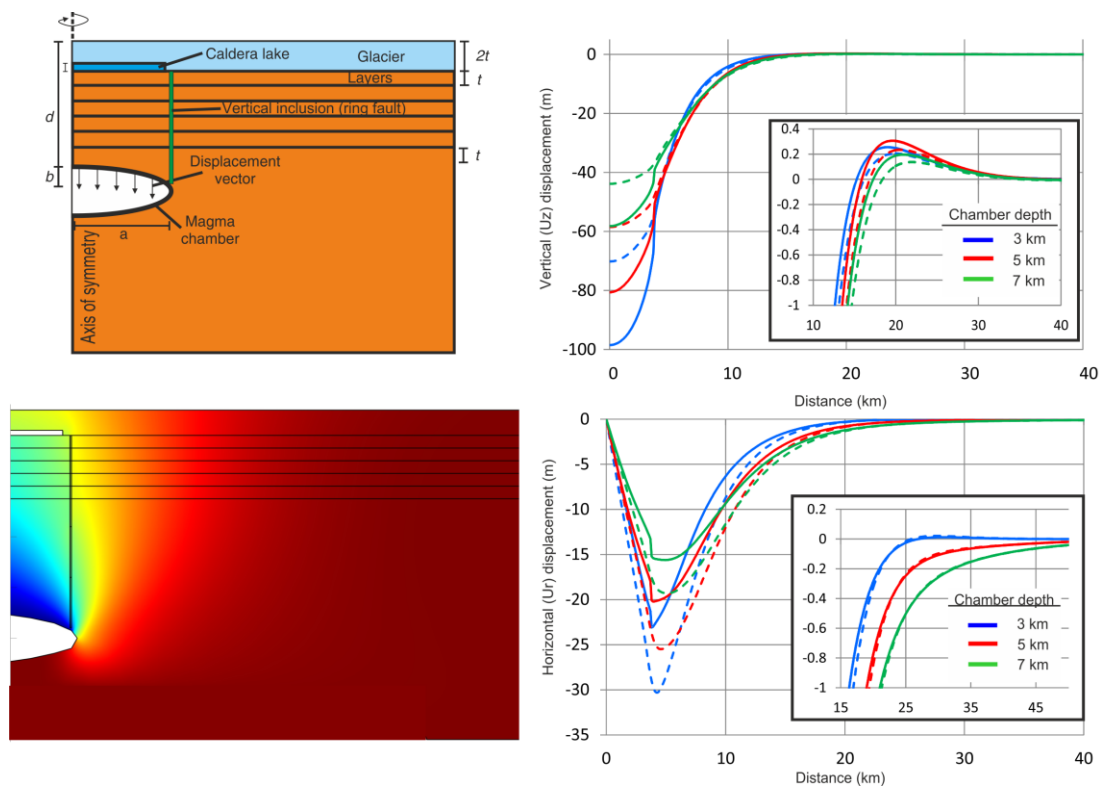
Fig. 10 Resultant displacements from a model which includes a soft (Young's modulus 1 GPa) fault zone, representing a ring-fault. In this model the crust is homogeneous and isotropic, i.e, not layered. Results are similar to those in models

without the weak fault zone, but differ in that surface subsidence is concentrated within a narrower region. Additionally, the crustal segment experiences a positive vertical displacement (~30 cm), inflation between around 15 and 20 km from the chamber centre. Chamber radius (a) is 4 km and half-thickness (b) is 1 km, depth below the surface (d) is 5 km.

5.2 Layered (anisotropic) crustal segment

Two layered crustal-segment models were run (Fig. 11). One model (A) has two soft layers in-between stiffer crustal units, while the other model (B) has three soft layers, including the top layer. All the soft layers have a stiffness of 1 GPa, which corresponds to the stiffnesses of soft hyalaoclastites (basaltic breccias) and of glacial sediments, such as are common in most active volcanoes in Iceland. The layers are modelled as soft to explore the maximum effects that sediments and soft breccias could have on the displacement fields. Introducing mechanical heterogeneities and anisotropies through soft layers with low Young's moduli into the model setup has the following effects:

- There is a general reduction in magnitudes of the far-field displacements. That is, the horizontal and vertical displacements far from the chamber/caldera centre are smaller in the layered models than in the non-layered models (Table 2).
- The maximum vertical displacements are also smaller in the layered models than in the non-layered models. More specifically, the maximum surface vertical displacements in the bedrock/crust are 79-84 m in the layered models but 97-98 m in the non-layered models (Table 2). Similarly, the maximum surface displacement in the ice in the layered models is 64-65 m, but 70-72 m in the non-layered models.
- The maximum horizontal surface displacements are much smaller in the layered models than in the non-layered models. In the layered models the maximum surface horizontal displacement is 2-6 m but 23-25 m in the non-layered models.

The general effect of layering is to reduce the displacements measured at the surface of the bedrock/crust and the ice. The reasons for the reductions are partly that the

stresses become "dissipated" at the contacts with the soft layers. Similar results have been obtained in general studies of surface deformation associated with various pressure sources, such as dykes (Gudmundsson, 2003). Crustal segments with alternating stiff and very soft layers generally transport less stress and deformation to the surface than non-layered segments, or segments where all the layers have similar mechanical properties. Well-known examples of the reducing effects of mechanically contrasting layers on surface stresses and deformation/displacement relate to emplacement of dykes and other vertically fluid-driven fractures (Gudmundsson, 2003; Philipp et al., 2013).
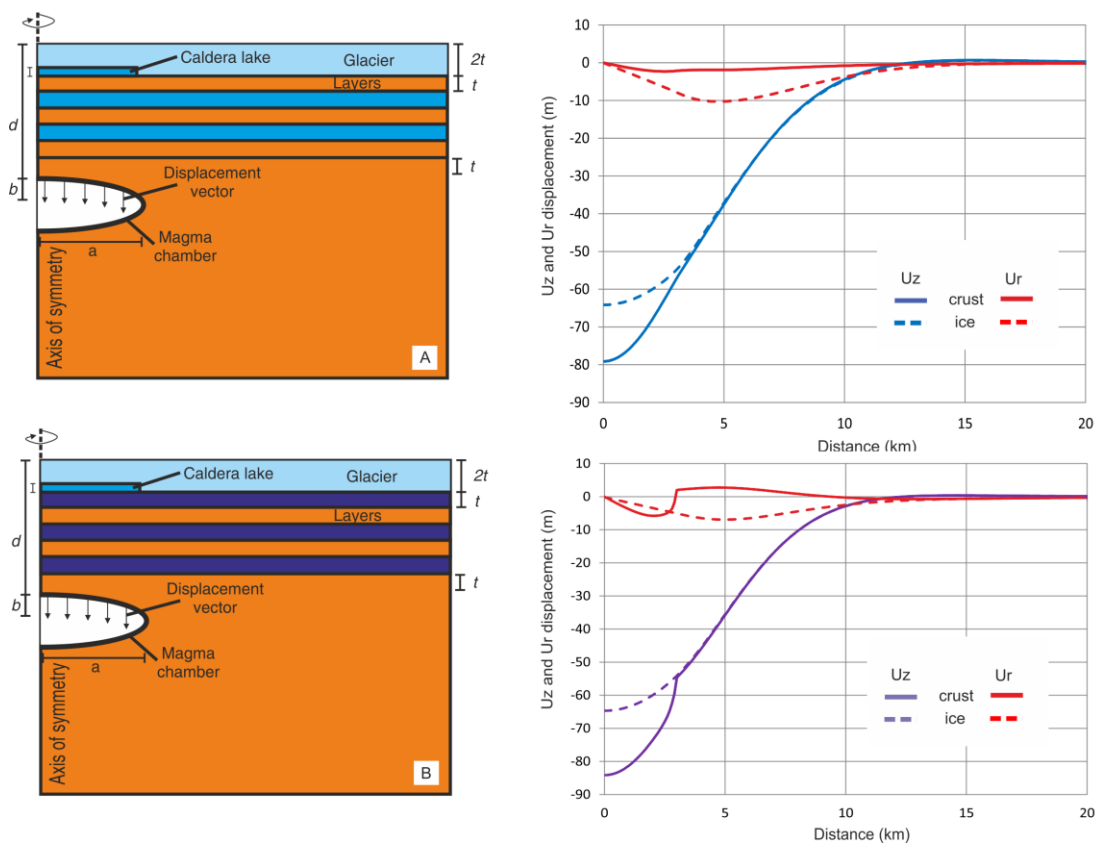
Fig. 11 Displacements generated through chamber-roof subsidence of 100 m in a layered crustal model. In the upper model (A), the layering is configured so that two soft layers (Young's modulus E = 1 GPa) lie in-between stiffer units which have the same Young's modulus as the crust. In the lower model (B) we add three soft layers in between crustal units, where the uppermost is in contact with the glacier. Coloured layers indicate soft hyaloclastite as material inputs shown in the model setups on the left. Graphs on the right indicate the vertical and horizontal displacements in the crustal (solid) and ice (dashed) surface for each layer configuration. Generally, there is a reduction in far-field displacements and the magnitude of local displacements is less in both model set-ups, compared to the previous homogeneous setups. Chamber radius (a) is 4 km and half-thickness (b) is 1 km, depth (d) is 5 km.

6. Ring-fault subsidence

We also modelled the effects of a piston-like subsidence along a ring-fault on the surface displacement fields. In view of the results from Bardarbunga, where inferred vertical maximum displacement in the ice inside the collapse caldera is about 60 m (Hench et al, 2015), we impose 50 m vertical displacement on the ring-fault (Fig. 12). The ring-fault, the fault zone, is modelled as a soft inclusion, with a Young's modulus of 0.1 GPa. We tried other stiffnesses for the fault, such as 0.01 GPa, but the overall results remained similar. The crust itself is non-layered in this model with the properties used in the earlier non-layered models (Table 1).

The results (Fig. 12) show that the displacement, both the vertical and the horizontal, becomes more concentrated at and within the caldera (the ring-fault) than in the previous roof-subsidence models without ring-fault. The maximum subsidence of the bedrock/crust is the same as that of the fault, namely 50 m, but the ice subsidence is greater, or 60 m. This is because the ice can bend or subside somewhat into the caldera lake at the contact between the ice and the crust, whereas the crust clearly cannot do so. For the same reason, the horizontal displacement (towards the centre) at the surface of the ice also exceeds that of the crust. Both reach a maximum at the location of the ring-fault, the vertical displacement of the ice (the fault throw) being up to about 17 m and that of the bedrock/crust up to 10 m.

These results illustrate various aspects of the effect of ring-fault subsidence in a caldera located beneath ice, including the following:

- The crustal displacements, the horizontal and, in particular, the vertical, reflect strongly the ring-fault geometry. This means that both displacements are maximum at the caldera fault. In fact, the vertical displacement reaches its maximum of 50 m at the fault and stays the same throughout the roof of the chamber.
- The caldera lake magnifies the surface displacement of the ice. The horizontal displacement in the ice is considerably larger than that in the crust. And, most importantly, the total vertical displacements in the ice exceed that imposed on the ring-fault by about 10 m. This is because of the caldera lake beneath the ice into which the ice can subside.

- Displacement of 50 m is so large that it would certainly cut through the ice as a fault. The inferred vertical displacement at the location of the ring-fault are about 17 m. No tensile or shear strength is given to ice in the model, so it does not fracture. But 50 m vertical displacement in an ice sheet of thickness, say, 800-1000 m would become very clearly through-faulted.
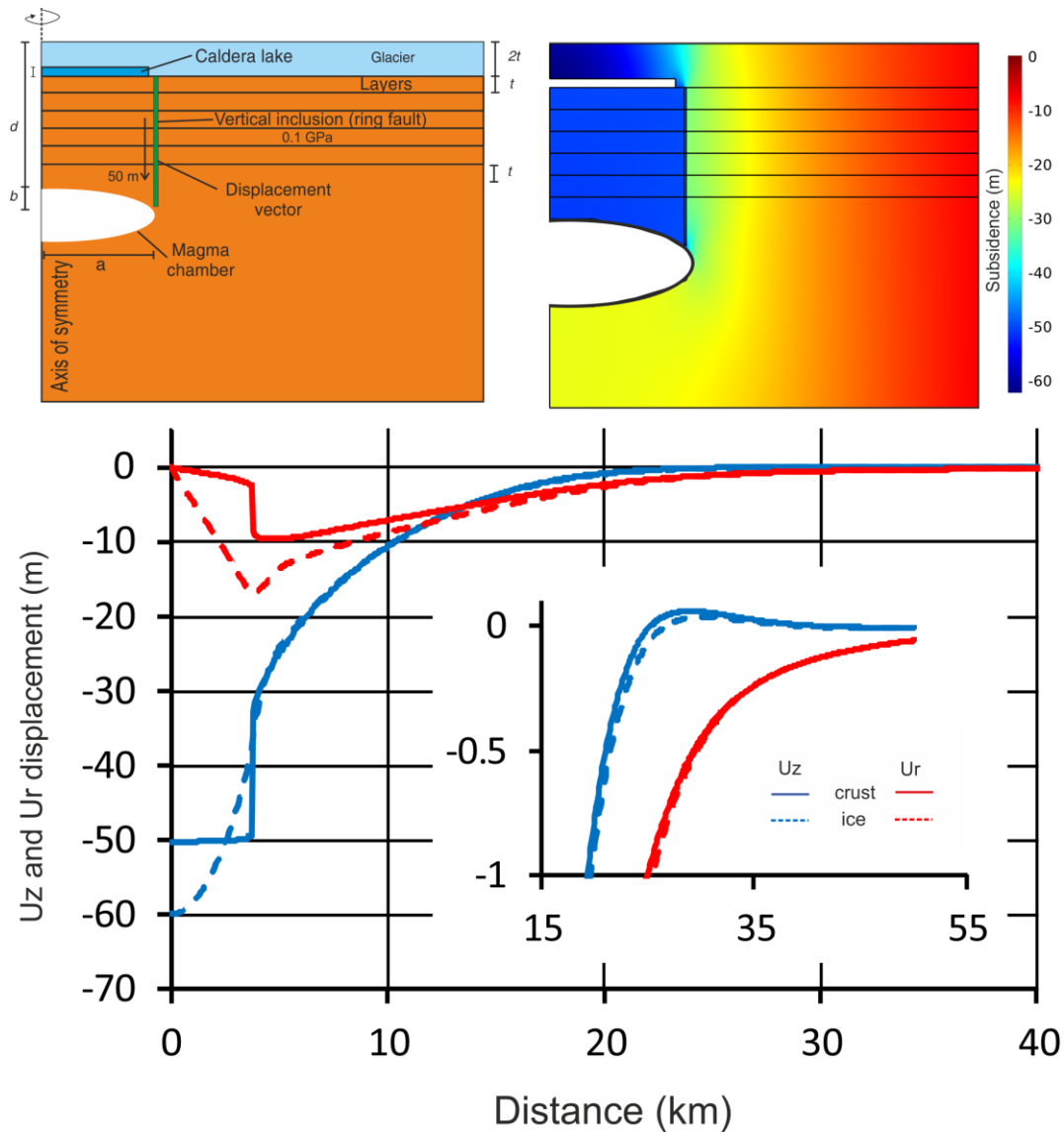
Fig. 12 Piston like vertical subsidence of 50 m along the inner edge (z-axis) of a ring-fault, a soft elastic zone which extends from the crustal surface to 3 km depth. The soft fault zone has a Young's modulus of 0.1 GPa and the crustal segment is homogeneous and isotropic. Displacements are highly focussed within the caldera region, with maximum vertical and horizontal displacement greatest in the ice surface. The caldera lake acts to magnify displacements within the ice, presumably because the ice is able to subside into the lake surface. Chamber radius (a) is 4 km and half-thickness (b) is 1 km, depth below the surface (d) is 5 km.

7. Discussion: Implications for the 2014-15 Bardarbunga-Holuhraun episode

The underpressure or withdrawal-of-magmatic-support model is often favoured when explaining the formation of calderas, both in analogue-model setups (Holohan et al., 2011; Acocella et al., 2000) and for explaining geophysical observations (Peltier et al., 2008; Kusumoto and Gudmundsson, 2009). Most recently this model has been invoked to explain ice surface subsidence above the Bardarbunga Caldera (Sigmundsson et al., 2015). The assumption is then that a volume of magma was removed from a chamber by lateral magma propagation, eventually forcing an eruption some 45 kilometres from the central volcano. Similar ideas have been offered to explain the occurrence of lavas outside the main central volcanoes and within the active rift zone of Iceland (Sigurdsson and Sparks, 1978), although more recent studies have shown that alternative explanations with predominating vertical magma propagation are equally plausible (Hartley and Thordarsson, 2012). The competing hypothesis is that the Holuhraun lavas, and many other large and rather primitive basaltic fissure eruptions in Iceland, are fed by regional dykes which are injected from magma reservoirs at a much greater depths (15-25 km) than the shallow chambers (Gudmundsson et al., 2014).

The models presented in this paper have certain implications for volcano-tectonic processes in central volcanoes in general. Further implications apply primarily to calderas located in ice sheets such as many calderas in Iceland - to Bardarbunga in particular. We consider first the implication for the magnitude of the surface displacements and the size of the area affected (the surface area showing significant displacement). Both aspects of the deformation are very important, particularly when trying to separate the deformation associated with a caldera and/or a shallow magma chamber from that associated with simultaneous dyke emplacement.

7.1 Surface displacements

Vertical surface displacements of 10-20 cm extend out to distances of 15-16 km from the centre of the caldera, and horizontal displacements of similar magnitude to 20-30 km (Fig. 8). For the horizontal displacement, 10 cm displacements occur out to 40-50 km from the centre, depending on the depth of the chamber. These refer to the non-layered models and the exact distances for the displacement mentioned

depend on the depth of the chamber: the surface displacements induced by the deepest chamber, at 7 km, extend for the greatest distances from the centre. If the surface displacement would relate partly to a deep-seated reservoir, as we propose here, say a reservoir at the depth of 15-20 km, then significant surface displacements would extend still further from the centre. Using the same model configuration and properties but roof-subsidence varying from 20 m to 100 m, the results are similar – significant displacements extend to 15-20 km from the centre (Fig. 13 A) and are only slightly less when a vertical ring-fault is introduced (Fig. 13 B).

The layered models produce less displacements, both in magnitude and lateral extension from the centre (Fig. 11). However, these models are with somewhat extreme layering since the soft layers have stiffness or Young's modulus of only 1 GPa, which is low for hyaloclastites and sedimentary rocks. Nevertheless, there are still large surface displacements of 50 cm at distances of about 12 km (for the vertical displacement) and 12-17 km (for the horizontal displacement) in the bedrock/crust, and somewhat larger distances in the ice (Table 2). Larger displacements are obtained from the 50-m-fault displacement model (Fig. 12).

Overall the displacement results indicate that, for the models considered, large displacements, of the order of tens of centimetres or hundreds of millimetres, should be detected out to distances of 10-20 km, for the vertical displacement, and 20-30 km or more for the horizontal displacements. Even for a small roof-subsidence of 20 m, the horizontal displacement at 10-12 km distance from the centre is still of the order of tens of centimetres (Fig. 13). Results of this kind show clearly the effect of nearby subsidence of a magma-chamber roof, or a collapse caldera displacement, and should make it possible to distinguish between displacements induced by such a subsidence and those induced by a dyke formed in the same volcano-tectonic episode.

The displacement field associated with the subsidence of the ice in the Bardarbunga episode in 2014-15 is educational in this respect. For the period up to 6 September 2014 the GPS-estimated maximum displacement or subsidence in the ice in the Bardarbunga Caldera was about 16 m (Sigmundsson et al., 2015), and the entire cumulative displacement during the episode 2014-15 is estimated at over 60 m (Hensch et al., 2015). Dyke emplacement was essentially completed by 31 August when the main eruption began (Gudmundsson et al., 2014; Sigmundsson et al.,

2015), and no significant horizontal dyke-induced displacements were detected after 4 September 2014 (Ofeigsson et al., 2015). The horizontal displacements induced by the dyke can thus largely be separated from those induced by the subsidence measured in the Bardarbunga Caldera.
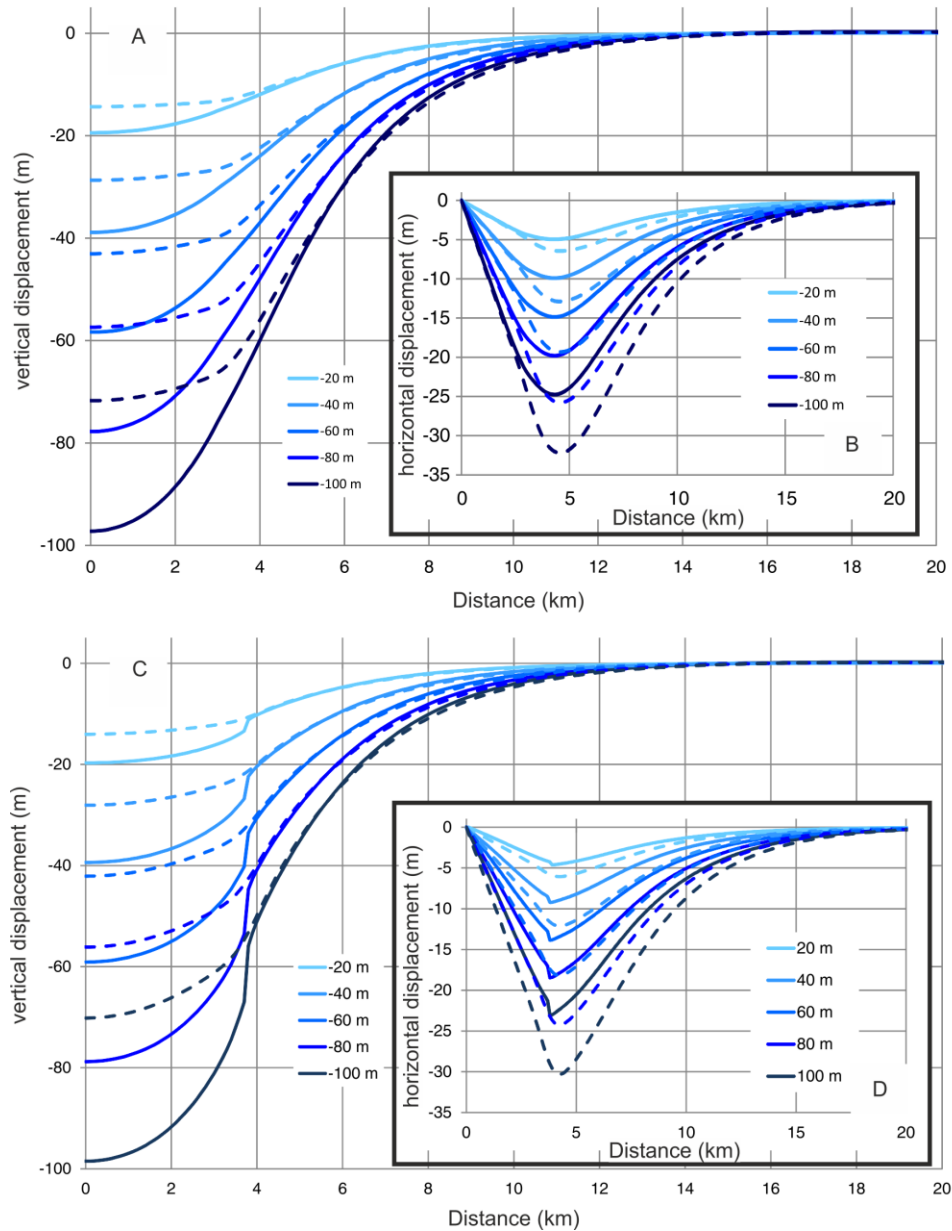
Fig. 13 Total vertical (A and C) and horizontal (B and D) displacements in crustal-surface (solid lines) and ice-surface (dashed lines) resulting from vertical chamber roof subsidence of between 20 and 100 m. Upper displacement curves (A and B) are from a homogeneous crustal model, whereas the lower curves (C and D) are from models which include a soft vertical zone, a ring-fault (C and D). The results are similar for both types of models, with slight variations in subsidence around the fault area. All models indicate significant far-field surface displacements, irrespective of the amount of roof subsidence. However, roof subsidence has a major control on the

local surface displacements directly above the magma chamber. In all model runs shown here chamber radius (a) is 4 km and half-thickness (b) is 1 km, with a chamber depth of 3 km.

Our model results suggest that vertical displacement of about 16-20 m, corresponding to period up to about 6 September, should generate horizontal displacements of the order of tens of centimetres towards the Bardarbunga Caldera within 10-12 km from the centre of the caldera. Similarly, horizontal displacements of many tens of centimetres are expected out to distances of up to tens of kilometres, depending on the model used – in particular, the assumed depth of the shallow chamber and mechanical properties of the host rock and the ring-fault. The measured displacements at the GPS stations in the crust outside the ice, some of which are at 13-17 km from the centre of the caldera, are significantly less than expected from the models (Sigmundsson et al., 2015; Ofeigsson et al., 2015). The difference may be partly related to the modelling procedure but most likely indicates that only part of the subsidence in the ice within the Bardarbunga Caldera is actually directly related the magma-chamber roof subsidence, or ring-fault displacement.

The last point is also of importance when interpreting the subsidence measured in the ice within the caldera. There are several remarkable features of the ice subsidence, as shown in maps by Sigmundsson et al. (2015), including the following:

- The maximum subsidence is about 3 km from the northern caldera rim and about 5 km from the southern and south-eastern rims.
- The subsidence at the rims, at the ring fault itself, is much smaller than the maximum subsidence – in fact about zero in the early stage of the subsidence.
- Fracture development at the surface of the ice is comparatively small, with no major caldera-related fault cutting through the ice.

These observations and measurements, when compared with the ring-fault subsidence model (Fig. 13), suggest the following interpretations. First, the displacement along the ring-fault is small in comparison with the overall subsidence in the ice. In particular, displacements of the order of 20-60 m along the ring fault would without doubt have propagated faults through the ice (say, vertical displacements of 10-20 m; Figs. 11 and 12) – and these faults are not observed. From

standard fracture mechanics (Gudmundsson, 2011) and the mechanical properties of a typical ice (Schulson and Duval, 2009; Table 2), a close-to vertical normal fault (Hensch et al., 2015) with displacement of up to tens of metres in ice of thickness of several hundred metres – in fact, the ice thickness is only 200-300 m above part of the caldera rims - would become a through crack, that is, reach the bottom and surface of the ice sheet. This conclusion is the same even if there is a caldera lake beneath the ice (Fig. 13). Since normal faults with these throws are not observed, the cumulative vertical ring-fault displacements cannot be of the of the order of tens of metres, and is most likely of the order of metres or less.

Second, for a porous-media chamber, as most chambers presumably are (Gudmundsson, 2012), the maximum subsidence, if caused by magma flow out of an underlying magma chamber, would normally be, initially at least, close to the 'outlet', that is, the intersection of the dyke or sheet transporting the magma with the boundary of the chamber. Sigmundsson et al. (2015) propose that the subsidence of the ice is directly related to chamber roof-subsidence associated with magma flowing laterally along a dyke that dissects a chamber along its southeast margin. It is not clear from the subsidence data, however, why the maximum subsidence is then not at the outlet but rather close to the northern margin of the chamber/caldera.

In fact, the inferred segmentation of the dyke, with distances between nearby tips of segments up to kilometres (Sigmundsson et al., 2015), is a strong argument against lateral flow of magma from a chamber beneath Bardarbunga and to the volcanic fissures in Holuhraun and an argument for vertical flow of magma from a deep-seated reservoir (Gudmundsson et al., 2014). The arguments against the lateral flow between dyke segments are many, including the following. (1) There is no seismicity between the nearby ends of some of the 8 segments, particularly between segments 1 and 2 and 5 and 6 (Sigmundsson et al., 2015, Extended Data Figure 2), suggesting that no magma migrated laterally between them. The zones connecting many of the segments, being highly oblique to the overall strike of the dyke, are zones of high shear stress making it highly unlikely that a magma-driven fractures could propagate along the zones without triggering earthquakes. Earthquakes are, in fact, used as criteria for identifying magma paths. It follows that absence of earthquakes, that is, seismically quiet zones, would normally mean absence of magma paths. (2) In the unlikely event of aseismic magma-path formation at shallow

depths from segment 1 to 2, and from segment 5 to 6, then the same magma would have to flow from the shallow depths vertically down to at least 10 km depth in segments 2 and 6. Downward flow of magma on this scale is not supported by any observations and does not agree with well-established physical principles of fluid dynamics and dyke propagation (Gudmundsson, 2011). Thus, the segments of the regional Bardarbunga-Holuhraun dyke were presumably formed primarily through vertical flow of magma from the proposed deep-seated magma reservoir (Gudmundsson et al., 2014).

7.2 Mechanisms for the ice and ring-fault subsidences

If excess magma pressure decrease in a shallow chamber is not the main cause of the subsidence in the ice in Bardarbunga, what alternative mechanisms exist? One obvious mechanism, well known from caldera studies, is slight doming or inflation of the volcanic field hosting a shallow magma chamber. Doming was in fact detected at GPS stations in a large area surrounding the Bardarbunga Caldera a few months before the unrest (Ofeigsson et al., 2015). Such a doming, as small as of the order of centimetres, is known to be one of the principal mechanisms for generating caldera collapses (Gudmundsson, 2007), particularly along normal ring-faults (Gudmundsson, 1998). Focal mechanisms suggest that the slip on the ring-fault of Bardarbunga in the 2014-15 episode was primarily through normal faulting (Bjarnason, 2014; Hensch et al., 2015; Riel et al., 2015). Most of the ring-fault seismicity occurred at shallow depths (<3 km) (Hjorleifsdottir et al., 2015), in agreement with the ring-fault seismicity being related to stress concentration above the margins of a proposed shallow magma chamber, as is the model suggested here (cf. Gudmundsson, 2007).

The doming or inflation of the volcanic field or system containing the Bardarbunga Caldera is most likely related to the associated deep-seated reservoir receiving new input of melt or magma. As doming begins, stress concentration at the ring-fault of the Bardarbunga Caldera results in subsidence – by how much we do not really know. The subsidence and associated faulting and possible ring-dyke formation (Gudmundsson et al., 2014) reduces the effective thickness of the crustal segment or plate above the shallow magma chamber (Figs. 5 and 9). The reduction in the effective plate thickness d_e encourages further doming of the volcanic field hosting

the Bardarbunga caldera even if the magmatic excess pressure at the deep-seated reservoir remains constant or decreases slightly for a while (Gudmundsson, 1998).

7.3 Relation between dyke emplacement and subsidence in the caldera

This last point brings us to the 45-km-long regional dyke and associated eruption, and how they relate to the subsidence in the Bardarbunga Caldera. The first thing to notice is that the strike of the dyke close to the caldera/chamber is in perfect agreement with the local trajectories of the maximum horizontal principal stress around a circular or slightly elliptical cavity under tension (Savin, 1961; Gudmundsson, 2011). Further from the chamber/caldera the regional stress field took over, and the dyke followed the field that has existed in this part of Iceland for at least 8-10 Ma (Gudmundsson et al., 2014). The main dyke was injected when the excess pressure in the deep-seated reservoir reached the conditions (Gudmundsson, 2011):

$$p_l + p_e = \sigma_3 + T_0 \tag{4}$$

where p_l is the lithostatic stress or overburden pressure at the reservoir rupture site (in the reservoir roof), $p_e = p_t - p_l$ is the difference between the total fluid pressure p_t in the reservoir and the lithostatic stress at the time of reservoir rupture, σ_3 is the minimum compressive or maximum tensile principal stress, and T_0 the local in situ tensile strength at the rupture site. When the dyke became injected into the roof of the reservoir and began to propagate up into the crustal layers above, its overpressure p_o changes as:

$$p_0 = p_e + (\rho_r - \rho_m)gh + \sigma_d \qquad ` \tag{5}$$

where p_e is the magmatic excess pressure in the reservoir at the time of rupture (and equal to the in-situ tensile strength of the roof at the rupture site, T_0), ρ_r is the host-rock density, ρ_m is the magma density, g is acceleration due to gravity, h is the dip dimension or height of the dyke above the rupture site, and σ_d is the differential stress at a particular depth in the crust (the depth of interest). At the magma-chamber rupture site itself, the stress difference is included in the excess pressure term, so that

there $\sigma_d = 0$. Also, at the rupture site, before the dyke has propagated and reached any significant height, we have $h = 0$, so that the third term in Eq. (5), the buoyancy term, becomes zero. It follows that the only pressure available to rupture the reservoir roof and drive the magma out at and close to the roof contact with the magma is the excess magmatic pressure p_e. We also know that $p_e = T_0$, that is, the excess pressure at the time of roof rupture is equal to the in-situ tensile strength, with in-situ (field) values ranging from 0.5 to 9 MPa (Amadei and Stephansson, 1997), the most common values being 2-4 MPa (Gudmundsson, 2011).

It follows that during the rupture and initial propagation of the resulting dyke, the only driving pressure is p_e, of the order of several mega-pascal. As the dip dimension (height) of the dyke increases, however, positive buoyancy adds to the driving pressure, so long as the average magma density is less than the average density of the rock layers through which the dyke propagates. The magma is olivine tholeiite (Haddadi et al., 2015) so that its density may be taken as about 2700 kg m^{-3} (Murase and McBirney, 1973). The erupted magma originated at depths somewhere between 10 and 20 km (Bali et al., 2014; Haddadi et al., 2015), that is, from a deep-seated magma reservoir as have been proposed under most volcanic systems in Iceland, and the Bardarbunga System in particular (Gudmundsson et al., 2014). Given the crustal density in Iceland, then from Eq. (5) the magmatic overpressure p_0 or driving pressure of the dyke, at different crustal depths (and thus with different σ_d values) could easily have reached 10-15 MPa (cf. Becerril et al., 2013; Gudmundsson et al., 2014).

In the model presented here, the injection of the main dyke from the deep-seated reservoir, as well as the subsidence in the Bardarbunga Caldera, were both the consequence of the same process: namely inflow of magma into the deep-seated reservoir. This inflow may have started many years before the 2014 episode, particularly from 2006 and onwards as indicated by seismcity (Vogfjörd et al., 2015), and was certainly noticeable as widespread doming or uplift on GPS instruments for months before the regional dyke injection began in August 2014 (Ofeigsson et al., 2015). There may have been magma flow into the shallow chamber associated with the caldera, and several smaller dykes may have been emplaced during the early stages of the episode – some from the deep-seated reservoirs, others

(small radial dykes) from the shallow chamber. The only dyke to develop into a major dyke, however, was the 45-km-long regional dyke emplaced over a period of 2 weeks in August 2014 (Gudmundsson et al., 2014; Sigmundsson et al., 2015).

The regional dyke presumably came from depths of at least 15-20 km, perhaps deeper. This is suggested partly by the chemistry of the erupted lavas (Bali et al., 2014; Haddadi et al., 2015), partly by the widespread doming detected in the months before the episode, discussed above, and partly by the earthquake distribution in the area. From 2012 there were many earthquakes north and northeast of the Bardarbunga Caldera (Vogfjörd et al., 2015), where one of the earthquake swarms (and possible dyke injection) occurred during the first days of the August 2014 episode. Even more importantly, deep earthquakes occurred in a vertical zone southeast of the Bardarbunga Caldera from about this time and extended until August 2014 (Vogfjörd et al., 2015) at roughly the location of the first segment of the regional dyke, as formed in the first days of the August 2014 episode.

The regional dyke had enormous stress effects on the Bardarbunga Caldera and, by implication, the associated shallow magma chamber (Gudmundsson et al., 2014). The stress field induced by the dyke around the caldera contributed to three important aspects of the 2014 episode; (1) normal faulting along the caldera ring-fault, (2) elongation of the caldera in a northeast-southwest direction, and (3) ductile deformation and flow of the ice, primarily inside the caldera.

Normal faulting is the dominating mechanism on the Bardarbunga ring-fault during the present episode (Bjarnason, 2014; Hensch et al., 2015; Riel et al., 2015). This is in agreement with the two main mechanisms of caldera slip proposed here, namely: (1) a combination of stresses concentrating at the ring-fault as a consequence of slight doming due to excess pressure increase in the deep-seated reservoir (Gudmundsson, 2007) and (2) dyke-induced stress concentration, particularly at the northern and southern sectors of the ring-fault (Gudmundsson et al., 2014). Both encourage normal faulting on the ring-fault itself, while the dyke-induced stresses also encourage strike-slip and reverse-faulting on differently oriented faults away from the ring-fault (Gudmundsson et al., 2014).

The elongation of the ring-fault in the northeast-southwest direction is due to the compressive and shear stresses that concentrate in the "breakout areas" around the

caldera (Gudmundsson et al., 2014). Elongation of collapse calderas due to "breakouts" is well known from other areas (Bosworth et al., 2003). The elongation would encourage flow of magma to the ring-fault in these sectors, possible ring-dyke formation – which may partly explain the common non-double couple earthquakes (Riel et al., 2015) - and contribute to the subsidence of the caldera roof. The main reason why the earthquake activity along the Bardarbunga Caldera has been so concentrated in the north and south parts of the caldera is presumably related to the dyke-induced stresses in these sectors (Gudmundsson et al., 2014).

While no attempts were made to measure or monitor ice flow in the ice-sheet cover of the Bardarbunga Caldera and its vicinity during the 2014-15 episode, such flow is likely to have occurred. During the emplacement of the regional dyke east and northeast of the caldera, the magmatic overpressure in the dyke (Eq. 5) may easily have reached 10-15 MPa. The dyke induced major displacements and thus stresses, within the caldera, and the high mountains of the caldera rim must have transmitted those compressive stresses (σ_H) from the dyke into the ice (Fig. 14). Depending somewhat on the strain rate, ice flows at pressures or stresses of less than 1 MPa, so that stresses of up to 10 MPa – somewhat diminishing with distance from the dyke - would certainly have caused flow in the ice within the caldera. The main flow would have been within the caldera because that is where the mountains are high – the caldera rim – and can thus most easily transmit the dyke-induced stresses to shallow levels in the ice sheet (Fig. 14). Since ice flows from higher to lower pressure, the dyke-induced stresses would have encouraged ice flow out of the caldera.

How much the ice flow may have contributed to the measured 60 m subsidence in the ice is unknown. The comparatively minor fracturing at the surface of the ice during its subsidence would suggest that the ice was flowing right up to the surface. Flow in the ice may have contributed significantly to the measured subsidence. In this model, the flow or creep or strain rate was highest just after the emplacement of the regional dyke, and then became gradually lower, as is typical for a creeping response to sudden load or displacement (here the dyke emplacement).

As the excess pressure p_e in the deep-seated reservoir declined, the doming-related ring-fault displacement also gradually decreased and, as p_e approached zero, the subsidence stopped altogether. It is clear that long before the eruption came to an end

on 27 February 2015 the earthquake activity associated with the Bardarbunga Caldera had greatly diminished. Also, the subsidence measured in the Bardarbunga Caldera ceased several weeks before the end of the eruption. These and other observations suggest that the pressure decrease in the deep-seated reservoir was partly responsible for the ring-fault slips and associated earthquakes.
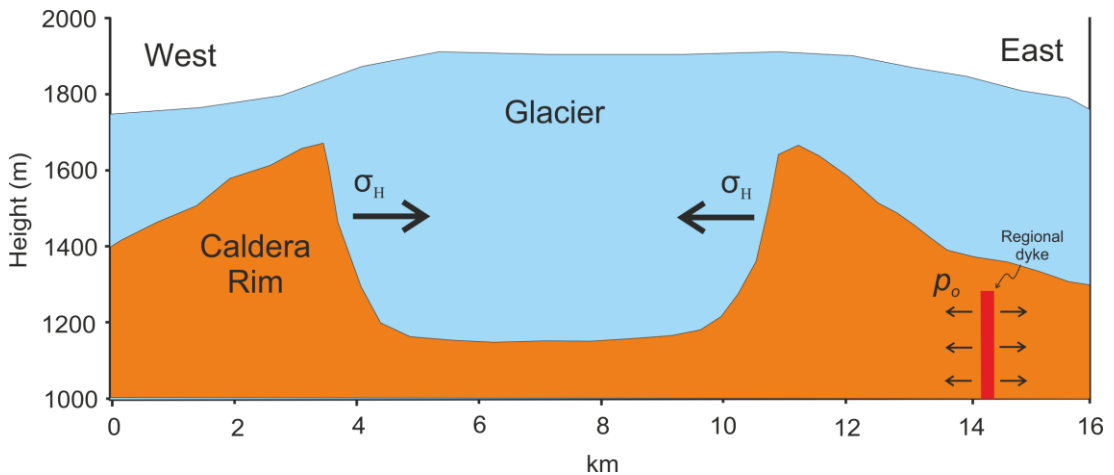
Fig. 14 A simplified E-W profile of the sub-glacial caldera at Bardarbunga volcanic system. Overpressure (p_o) from a regional dyke emplaced to the east of the caldera rim imposes large horizontal compressive stresses (σ_H) on the high caldera walls. The compression acts to squeeze ice within the caldera, making the ice behave as ductile up to the surface, and leading to increased ice flow out of the caldera. The resulting ice flow is likely to have contributed largely, perhaps dominantly, to the measured ice subsidence at Bardarbunga. The regional dyke is not to scale in this diagram and the sub-glacial caldera topography is a representation of the likely topographic setting of Bardarbunga, modified from Bjornsson, 1988.

8. Conclusions

We present general numerical models on the effects of "shallow" magma chamber contraction at various depths, namely the result of chamber roof subsidence at depths of 3 km, 5 km, and 7 km. In all the models, the magma chambers are associated with a collapse caldera which is located beneath a thick glacier or ice sheet. The models are general, and apply to many volcanoes in Iceland and elsewhere, but the results are here applied to the 2014-15 volcano-tectonic episode in Bardarbunga-Holuhraun in Iceland.

Several models were tested for the shrinkage of the magma chamber through vertical downward displacement of its roof. Some of the models use a simple elastic crust

(elastic half space) hosting the chamber, with an ice sheet on the top. Others use layered (anisotropic) crust above the shallow magma chamber, that is, layers with different stiffnesses (Young's moduli). And still other models have a caldera lake between the ice sheet and the rock or crustal surface. The simplest loading used is 100 m vertical downward displacement of the chamber roof. Other models include different vertical displacement of the roof (in steps from 20 m to 100 m), as well as displacement of 50 m along a vertical caldera fault (the ring-fault). Some of the main results are as follows:

- For chamber-roof displacements in the range of 20-100 m, the models suggest large vertical and particularly horizontal displacements in the ice and in the bedrock/crust surface under the ice out to distances of 10-40 km from the caldera centre, depending on the depth of the chamber and the exact type of modelling used. The vertical displacements in all models reach maximum at the surface of the bedrock/crust and the surface of the ice right above the centre of the subsiding magma-chamber roof. The horizontal displacements at the surface, however, reach their maximum values (maximum displacement towards the chamber or caldera centre) at a distance of 4-5 km from the centre.

- For a non-layered (isotropic) crustal model with a 100 m roof subsidence, the vertical displacement exceeds 50 cm to a distance of 14 km from the centre and the horizontal displacement exceeds 50 cm to a distance of 19 km from the centre. A chamber located at 3 km depth produces horizontal displacement of 20 cm to a distance of 21 km from the centre, and for a chamber at 7 km depth horizontal displacement of 20 cm is produced to a distance of 33 km from the centre. Similar results are obtained if a vertical non-slipping ring-fault is added to the model, but the displacements show an abrupt change (a break) at the location of the fault.

- The general effect of crustal layering (using mechanically layered or anisotropic models) is to reduce the displacements measured at the surface in comparison with those generated in the non-layered (isotropic) models. The reasons are partly that the stresses become 'dissipated' at contacts between still and soft layers.

In a model where the subsidence is related to vertical downward piston-like displacement by 50 m of the ring-fault, the results show that the vertical displacement in the crust/chamber roof exactly reflects that of the ring-fault and reaches a maximum of 50 m. By contrast, the vertical displacement in the ice follows a curve that reaches its maximum of 60 m in the centre of the caldera. This 'extra' vertical displacement in the ice is partly because it can bend or subside somewhat into the caldera lake below. Displacement of 50 m along the ring-fault is so large that the fault would most definitely cut through the ice, forming a through fault with displacements of up to tens of meters (which is not observed in Bardarbunga, however).

The modelling results have several implications for the interpretation of the 2014-15 Bardarbunga-Holuhraun episode.

- First, the measured horizontal displacements in the surface rocks outside the ice appear to be significantly less than expected from modelling 60 m vertical displacement. At stations west of the Bardarbunga Caldera, horizontal displacements towards the caldera of the order of tens of centimetres would be expected but are not observed. This indicates that the vertical displacement in the bedtrock/crust, and thus the chamber roof-subsidence, is significantly less than than the maximum of about 60 m measured in the ice.

- Second, a 50 or 60 m piston-like displacement along the ring-fault is ruled out. The ring-fault would, for such a large displacement, definitely cut through the ice to form a large and easily visible fault, but this has not happened. By contrast, there has been comparatively little fracturing in the ice within the Bardarbunga Caldera during the subsidence, which suggests that the ice behaved as ductile, was flowing, right up to its surface. The results seem to limit the actual ring-fault (piston-like) subsidence to, at most, a few metres.

- Which brings us to the third implication, namely that the 45-km-long regional dyke generated compressive stresses in the ice within the caldera which resulted in ice flow out of the caldera, thereby contributing to the measured subsidence in the ice. How large factor the ice flow may have been is unknown since no measurements of the ice flow were made. What is

known, however, is that ice flows easily at low pressures, of the order of 1 MPa, and our calculations suggest magmatic overpressure in the regional dyke of the order of 10-15 MPa.

We interpret the geochemical, seismic, and geodetic data so that the regional dyke was injected from a large reservoir at 15-20 km depth, perhaps deeper. Earthquake data suggest that the reservoir received new magma over many years before the beginning (in August 2014) of the Bardarbunga-Holuhraun episode, particularly from the year 2006 and onwards. The magma injection resulted in widespread doming (uplift), as detected by GPS instruments in the months prior to August 2014 when the dyke emplacement began (Ofeigsson et al., 2015).

In our interpretation, the August 2014 reservoir rupture and regional dyke injection as well as the ring-fault displacement (caldera subsidence) are both the consequence of the associated reservoir magmatic pressure increase and doming. The conditions for reservoir rupture, dyke injection, as well as the overpressure change with vertical propagation of the dyke, are presented in Eqs. (4) and (5). The effects of ring-fault formation or reactivation as a result of reservoir-pressure increase, slight doming, and stress concentration around the chamber/caldera are discussed in the paper with reference to earlier numerical models (Gudmundsson, 1998, 2007), all of which suggest doming as a main mechanism of ring-fault displacement. This mechanism is also in agreement with the dominating normal-fault focal mechanisms of the ring-fault earthquakes (Bjarnason, 2014; Hensch et al., 2015; Riel et al., 2015).

We interpret the seismic and geodetic data so that, in addition to the 45-km-long regional dyke, there may have been several other dyke injections, including a northwest-striking dyke emplaced some 15 km north of the caldera and several smaller radial dykes/inclined sheets injected from the shallow chamber beneath the caldera. The shallow chamber may have received magma from the reservoir during the episode before the radial dyke injection; alternatively, stress concentration around the shallow chamber, through the external loading (doming), can have triggered the radial dyke injection (Gudmundsson et al., 2014).

The regional dyke induced stress concentration at the caldera/shallow chamber, in addition to that generated by the doming. The dyke-induced stress concentration contributed to three processes during the 2014-15 episode. First, normal-fault slip

along the ring-fault. Focal mechanisms indicate dominating normal-fault slip along the ring-fault (Bjarnason, 2014; Hensch et al., 2015; Riel et al., 2015). Much of the faulting occurred at the northern and southern sectors of the ring-fault, exactly in the areas where numerical and analytical models suggest that dyke-induced stress encourages normal faulting (Gudmundsson et al., 2014). Second, caldera elongation and "breakout" mechanisms at the northern and southern sectors of the caldera/chamber were induced by the dyke. These may have encouraged ring-dyke emplacement. Third, ductile deformation and flow in the ice inside the caldera. The caldera rim is composed of tall mountains that transmitted the compressive stress induced by the dyke to the ice, resulting in ice flow out of the caldera. The rate of flow of ice was greatest immediately following the dyke emplacement, and then gradually declined, as is typical of creeping material response to a sudden load (here the dyke emplacement). How much the ice flow contributed to the measured 60-m-subsidence in the ice is as yet unknown.

As the excess pressure in the reservoir p_e decreased below a certain level, the stress concentration around the ring-fault became too small for further significant to large slips and associated earthquakes to occur. This follows because the main slips were through normal faulting, so that the slips were controlled by the available driving stress at any time. Thus both the ice flow and the ring-fault subsidence gradually decreased with time. Significant subsidence in the caldera had apparently stopped in early February, several weeks before the eruption in Holuhraun came to an end on 27 February 2015. That the eruption continued for several more weeks indicates that it ceased only when the excess pressure in the deep-seated reservoir had vanished completely, that is, its excess pressure p_e had become zero.

Acknowledgements

9. References

Acocella, V., Cifelli, F. and Funiciello, R., 2000. Analogue models of collapse calderas and resurgent domes, *Journal of Volcanology and Geothermal Research*, 1-4, 81–96.

Acocella, V. 2007. Understanding caldera structure and development: An overview of analogue models compared to natural calderas, *Earth-Science Reviews*, 85, 125–160.

Amadei, B and Stephansson,O. 1997. *Rock Stress and its Measurement*. Chapman and Hall, New York

Anderson E.M., 1937. The dynamics and formation of cone-sheets, ring dikes, and cauldron-subsidence. *Royal Society of Edinburgh Proceedings,* 128–157

Bali, E., Gudfinnsson, G.H., Gunnarsson, H., Halldorsson, S.A., Jakobsson, S., Riishuus, M.S., Sigmarsson, O., Sigurdsson, G., Sverrisdottir, G., and Thordarson, T., 2014. Petrology of the new fissure eruption north of Dyngjujökull. *Geoscience Society of Iceland, Autumn Meeting 2014, Reykjavik*, pp. 5-6.

Bjarnason, I. 2014. Earthquake sequence 1973-1996 in Bardarbunga volcano: seismic activity leading up to eruptions in the NW-Vatnajokull area. *Jokull*, 64, 61-82.

Björnsson, H. 1988. *Hydrology of ice caps in volcanic regions*. Societas Scientarium Islandica, University of Iceland.

Becerril, L., Galindo, I., Gudmundsson, A., Morales, J.M., 2013. Depth of origin of magma in eruptions. *Scientific Reports*, 3, 2762, doi: 10.1038/srep02762

Bosworth, W., Burke, K., Strecker, M., 2003. Effect of stress fields on magma chamber stability and the formation of collapse calderas. *Tectonics*, 22, doi: 10.1029/2002TC001369

Browning, J. and Gudmundsson, A. 2015. Caldera faults capture and deflect inclined sheets: an alternative mechanism of ring dike formation, *Bulletin of Volcanology*, 77, 1-13. doi: 10.1007/s00445-014-0889-4

Cole, J. 1990. Structural control and origin of volcanism in the Taupo volcanic zone, New Zealand. *Bulletin of Volcanology,* 52, 445-459 doi: 10.1007/BF00268925

Cole, J., Milner, D. and Spinks, K. 2005. Calderas and caldera structures: a review. *Earth-Science Reviews*, 69, 1–26, doi: 10.1016/j.earscirev.2004.06.004

Deb, D., 2006. *Finite Element Method: Concepts and Applications in Geomechanics*. Prentice-Hall, New York.

De Natale, G. and Pingue, F. 1993. Ground deformations in collapsed caldera structures, *Journal of Volcanology and Geothermal Research*, 57, 19–38.

Druitt, T. and Sparks, R.S.J., 1984. On the formation of caldera during ignimbrite eruptions, *Nature*, 310, 679–681.

Folch, A. and Martí, J. 2004. Geometrical and mechanical constraints on the formation of ring-fault calderas, *Earth and Planetary Science Letters*, 221, 215–225.

Fritz, W.J., Howells, M.F., Reedman, A.J., Campbell, S.D.G. 1990. Volcaniclastic sedimentation in and around an Ordovician subaqueous caldera, Lower Rhyolitic Tuff Formation, North Wales. *Geological Society of America Bulletin*, 78, 1246-1256. doi: 10.1130/0016-7606

Gammon, P.H., Kiefte, H., Clouter, M.J. and Denner, W.W. 1983. Elastic constants of artificial and natural ice samples by Brillouin spectroscopy. *Journal of Physical Chemistry*, 29, 433–460. doi: 10.1021/j100244a004

Geshi, N., Shimano, T., Chiba, T., Nakada, S. 2002. Caldera collapse during the 2000 eruption of Miyakejima Volcano, Japan. *Bulletin of Volcanology*, 64, 55–68. doi: 10.1007/s00445-001-0184-z

Geyer, A. and Bindeman, I. 2011. Glacial influence on caldera-forming eruptions, *Journal of Volcanology and Geothermal Research,*. 202, 127–142.

Geyer, A., Folch, A. and Martí, J. 2006. Relationship between caldera collapse and magma chamber withdrawal: An experimental approach. *Journal of Volcanology and Geothermal Research*, 157, 375–386

Geyer, A., and Gottsmann, J 2010. The influence of mechanical stiffness on caldera deformation and implications for the 1971–1984 Rabaul uplift (Papua New Guinea). *Tectonophysics,* 483, 399–412. doi: 10.1016/j.tecto.2009.10.029

Gray, J.P. and Monaghan, J.J. 2004. Numerical modelling of stress fields and fracture around magma chambers, *Journal of Volcanology and Geothermal Research*, 135, 259–283.

Gregg, P.M., De Silva, S.L., Grosfils, E.B. and Parmigiani, J.P. 2012. Catastrophic caldera-forming eruptions: Thermomechanics and implications for eruption triggering and maximum caldera dimensions on Earth, *Journal of Volcanology and Geothermal Research*, 241-242, 1–12, doi: 10.1016/j.jvolgeores.2012.06.009

Grosfils, E.B., McGovern, P.J., Gregg, P.M., Galgana, G. A., Hurwitz, D.M., Long, S.M. and Chestler, S.R. 2015. Elastic models of magma reservoir mechanics: a key tool for investigating planetary volcanism. *Geological Society of London, Special Publications*, doi:10.1144/SP401.2.

Gudmundsson, A. 1998. Formation and development of normal-fault calderas and the initiation of large explosive eruptions. *Bulletin of Volcanology*, 60, 160–171, doi: 10.1007/s004450050224

Gudmundsson, A., 2003. Surface stresses associated with arrested dykes in rift zones. *Bulletin of Volcanology*, 65, 606-619, doi: 10.1007/s00445-003-0289-7

Gudmundsson, A. 2007. Conceptual and numerical models of ring-fault formation. *Journal of Volcanology and Geothermal Research*, 164, 142–160.

Gudmundsson, A., 2011. *Rock Fractures in Geological Processes*. Cambridge University Press, Cambridge.

Gudmundsson, A. 2012 Magma chambers: formation, local stresses, excess pressures, and compartments. *Journal of Volcanology and Geothermal Research*, 237-238, 19–41.

Gudmundsson, A., 2014. Elastic energy release in great earthquakes and eruptions. *Frontiers in Earth Science*, 2, 10, doi:10.3389/feart.2014.00010

Gudmundsson, A., 2015. Collapse-driven large eruptions. *Journal of Volcanology and Geothermal Research,* 304, 1-10, doi: 10.1016/j.jvolgeores.2015.07.033

Gudmundsson, A., Lecoeur, N., Mohajeri, N., and Thordarson, T., 2014. Dike emplacement at Bardarbunga, Iceland induces unusual stress changes, caldera deformation, and earthquakes. *Bulletin of Volcanology*, 76, 1–7, doi: 10.1007/s00445-014-0869-8

Gudmundsson, M.T., Sigmundsson, F. and Björnsson, H. 1997, Ice–volcano interaction of the 1996 Gjálp subglacial eruption, Vatnajökull, Iceland, *Nature*, 389, 954–957.

Gudmundsson, M.T, Sigmundsson, F., Björnsson, H., Högnadóttir, T., 2004. The 1996 eruption at Gjálp, Vatnajökull ice cap, Iceland: efficiency of heat transfer, ice deformation, and subglacial water pressure. *Bulletin of Volcanology*, 66, 46–65, doi:10.1007/s00445-003-0295-9

Gudmundsson, M.T., Thordarson, T., Höskuldsson, A., Larsen, G., Björnsson, H., Prada, F.J., Oddsson, B., Magnusson, E., Högnadottir, T., Petersen, G.N., Hayward, C.L., Stevenson, J.A., and Jonsdottir, I., 2012. Ash generation and distribution from the April-May 2010 eruption of Eyjafjallajökull, Iceland. *Scientific Reports*, 2, doi:10.1038/srep00572

Haddadi, B., Sigmarsson, O., Devidal, J. L. 2015. Determining intensive parameters through clinopyroxene-liquid equilibrium in Grímsvötn 2011 and Bárðarbunga 2014 basalts. *Geophysical Research Abstracts*, 17, EGU2015-5791-2

Hartley, M.E. and Thordarson, T. 2012, Formation of Oskjuvatn caldera at Askja, North Iceland: Mechanism of caldera collapse and implications for the lateral flow hypothesis, *Journal of Volcanology and Geothermal Research*, 227-228, 85–101.

Hensch, M., Cesca, S., Heimann, S., Rivalta, E., Hjörleifsdottir, V., Jonsdottir, K., Vogfjörd, K., Dahm, T. and the SIL Earthquake Monitoring Team, 2015. Earthquake focal mechanisms associated with the dyke propagation and caldera collapse at the Bardarbunga volcano, Iceland. *Geophysical Research Abstracts*, 17, EGU2015-5854-1.

Hickey, J. and Gottsmann, J. 2014. Benchmarking and developing numerical Finite Element models of volcanic deformation, *Journal of Volcanology and Geothermal Research*, 280, 126–130.

Holohan, E.P., Troll, V.R., Walter, T.R., Münn, S., McDonnell, S. and Shipton, Z.K. 2005. Elliptical calderas in active tectonic settings: an experimental approach, *Journal of Volcanology and Geothermal Research*, 144, 119–136.

Holohan, E.P., Schöpfer, M.P.J. and Walsh, J.J. 2011. Mechanical and geometric controls on the structural evolution of pit crater and caldera subsidence, *Journal of Geophysical Research*. 116, doi: 10.1029/2010JB008032

Hjörleifsdóttir, V., Jónsdóttir, K., Hensch, M., Guðmundsson, G., Roberts, M., Ófeigsson, B., and M. T., Gudmundsson, M. 2015. Numerous large and long-duration seismic events during the Bárðarbunga volcanic eruption in 2014: What do they tell us about the caldera subsidence? *Geophysical Research Abstracts*, 17, EGU2015-8143-1EGU

Kennedy, B., Stix, J., Vallance, J.W., Lavallée, Y. and Longpré, M.A. 2004. Controls on caldera structure: Results from analogue sandbox modeling, *Geological Society of America Bulletin*. 116, 515, doi: 10.1130/B25228.1

Kinvig, H.S., Geyer, A. and Gottsmann, J. 2009. On the effect of crustal layering on ring-fault initiation and the formation of collapse calderas, *Journal of Volcanology and Geothermal Research*, 186, 293–304.

Kusumoto, S., and Gudmundsson, A., 2009. Magma-chamber volume changes associated with ring-fault initiation using a finite-sphere model: application to the Aria caldera, Japan. *Tectonophysics*, 471, 58-66, doi: 10.1016/j.tecto.2008.09.001

Lavallée, Y., Stix, J., Kennedy, B., Richer, M. and Longpré, M.A. 2004. Caldera subsidence in areas of variable topographic relief: results from analogue modeling, *Journal of Volcanology and Geothermal Research*, 129, 219–236.

MacDonald, G.A., 1965. Hawaiian calderas. *Pacific Science,* 19, 320-334

Marti, J., Geyer, A., Folch, A. 2009, A genetic classification of collapse calderas based on field studies and analogue and theoretical modelling, in *Volcanology: the Legacy of GPL Walker, eds T. Thordarson and S. Self* (London: IAVCEI-Geological Society of London), 249–266.

Manconi, A., Walter, T.R. and Amelung, F. 2007. Effects of mechanical layering on volcano deformation, *Geophysical Journal International*, 170, 952–958, doi: 10.1111/j.1365-246X.2007.03449.x

Masterlark, T., 2007. Magma intrusion and deformation predictions: sensitivities to the Mogi assumptions. *Journal of Geophysical Research*, 112, 6419, doi: 10.1029/2006JB004860

Michon, L., Massin, F., Famin, V., Ferrazzini, V., & Roult, G. 2011. Basaltic calderas: Collapse dynamics, edifice deformation, and variations of magma withdrawal. *Journal of Geophysical Research,* 116, doi: 10.1029/2010JB007636

Mogi, K., 1958. Relations between eruptions of various volcanoes and the deformations of the ground surfaces around them. *Bulletin of the Earthquake Research Institute*. 36, 99–134.

Murase, T. and McBirney, A.R., 1973. Properties of some common igneous rocks and their melts at high temperatures. *Geological Society of America Bulletin*, 84, 3563-3592,

Ofeigsson, B.G., Hreinsdottir, S., Sigmundsson, F., Fridriksdottir, H., Parks, M., Dumont, S., Arnadottir, T., Geirsson, H., Hooper, A., Roberts, M., Bennett, R., Sturkell, E., Jonsson, S., Lafemina, P., Jonsson, T., Bergsson, B., Kjartansson, V., Steinthorsson, S., Einarsson, P., and Drouin, V., 2015. Deformation derived GPS geodesy associated with Bardarbunga 2014 rifting event in Iceland. *Geophysical Research Abstracts*, 17, EGU2015-7691-4.

Paterson, W.SB. 1994. *The Physics of Glaciers*, Pergamon/Elsevier, Kidlington. 480 pp, 3rd edition

Parameswaran, V. 1987. Orientation Dependence of Elastic Constants for Ice, *Defence Science Journal*. 37, 367–375, doi:10.14429/dsj.37.5924

Peltier, A., Famin, V., Bachèlery, P., Cayol, V., Fukushima, Y., & Staudacher, T. 2008. Cyclic magma storages and transfers at Piton de La Fournaise volcano (La Réunion hotspot) inferred from deformation and geochemical data. *Earth and Planetary Science Letters*, 270, 180-188.

Philipp, S.L., Afsar, F. and Gudmundsson, A., 2013. Effects of mechanical layering on hydrofracture emplacement and fluid transport in reservoirs. *Frontiers in Earth Sciences*, 1**,** doi: 10.3389/feart.2013.00004

Phillipson, G., Sobradelo, R. and Gottsmann, J. 2013, Global volcanic unrest in the 21st century: An analysis of the first decade. *Journal of Volcanology and Geothermal Research*. 264, 183–196.

Riel, B., Milillo, P., Simons, P., Lundgren, P., Kanamori, H., Samsonov, S., 2015. The collapse of Bardarbunga caldera, Iceland. *Geophysical Journal International,* 202, 446-453, doi: 10.1093/gji/ggv157

Roche, O., Druitt, T.H. and Merle, O. 2000, Experimental study of caldera formation, *Journal of Geophysical Research*, 105, 395, doi: 10.1029/1999JB900298

Savin, G.N., 1961. *Stress Concentration Around Holes*. Pergamon, New York.

Schulson, E.M. and Duval, P., 2009. *Creep and Fracture of Ice*. Cambridge University Press, Cambridge.

Sigmundsson, F., Hooper, A., Parks, M., Spaans, K., Gudmundsson, G.B., Drouin, V., Samsonov, S., White, R.S., Hensch, M., Pedersen, R., Bennett, R.A., Greenfield, T., Green, R.G., Sturkell, E., Bean, C.J., Mo, M., Femina, P.C. La, Bjo, H., Pa, F., Braiden, A.K., Eibl, E.P.S., 2015. Segmented lateral dyke growth in a rifting event at Barðarbunga volcanic system, Iceland. *Nature*, 517, 191–195.

Sigurdsson, H., and Sparks, S. R. 1978. Lateral magma flow within rifted Icelandic crust. *Nature*, 274, 126-130

Stix, J., and Kobayashi, T., 2008. Magma dynamics and collapse mechanisms during four historic caldera-forming events. *Journal of Geophysical Research* 113, doi:10.1029/2007JB005073

Vogfjörd, K., Hensch, M., Hjörleifsdottir, V. and Jonsdottir, K., 2015. High-precision mapping of seismicity in the last decades at Bardarbunga volcano, Iceland. *Geophysical Research Abstracts*, 17, EGU2015-13430-2

Williams, H., 1941. Calderas and their origin, University of California Publications. *Bulletin of the Department Geological Science* 25, 239–346.

Zienkiewicz, O.C. 1979. *The Finite Element Method*, McGraw-Hill, New York, 787 pp